Comprehensive characterization of a cost-effective Microbial Fuel Cell with Pt-free catalyst cathode and slip-casted ceramic membrane

Jesús Rodríguez[1*], Laura Mais[2], Roberto Campana[1], Lorenza Piroddi[1,2], Michele Mascia[2], Jonas Gurauskis[3], Annalisa Vacca[2], Simonetta Palmas[2]

[1]Centro Nacional del Hidrógeno, Puertollano, 13500, Spain

[2]Università degli studi di Cagliari, Dipartimento di Ingegneria Meccanica, Chimica e dei Materiali, Cagliari, 09123, Italy

[3]ARAID Foundation, Aragón Nanoscience and Materials Institute (CSIC-Unizar), Zaragoza, E-50009, Spain

*corresponding author (jesus.rodriguez@cnh2.es)

Abstract

This work reports a new procedure for low-cost Microbial Fuel Cells (MFCs) manufacture, based on the optimization of the most expensive MFC components: separator and cathode. For the first time, tubular MFC clay separators were fabricated by slip-casting, which allowed to reach the lowest thickness reported to date (1.55 mm), with a minimum cost (0.43 €·m^{-2}). On the other hand, a novel cathode was fabricated by using commercial CuO based catalyst and Carbon Mesh (CM). The new cathode showed a power density of 110 mW·m^{-2}, more than 40 % higher than other Cu based cathodes for Ceramic-MFCs (C-MFCs) studied in the literature. The proposed cell was operated for more than 6 months, with a power reduction of 29.4%, contrasting with Pt-cathodes (deactivation of almost 50% during the first month). A deep economic analysis showed a cost of 0.49€/cell when energetic optimization and a semi-industrial production were considered, one of the lowest for C-MFCs ever reported.

Keywords: Low-cost Microbial fuel cell; Ceramic separator, Slip-Casting, Pt-free cathode; Copper oxide catalyst

1. Introduction

Nowadays, it is beyond all doubt that Microbial Fuel Cells (MFCs) will be a future technology to address the climate change mitigation challenge [1]. Their greatest potential lies in their ability to transform the energy stored in wastewater into electricity, thanks to the action of exoelectrogens [2], able to perform simultaneously wastewater treatment and clean energy production. Furthermore, using waste as a raw material is one of the fundamentals of the Circular Economy empowering MFC concept potential even further.

However, the development of MFCs is limited by their high production costs, which represents a key aspect for their effective industrial application [3]. The mayor cost contribution corresponds to membrane and cathode which may be estimated to account to 47% and 38%, respectively [4]. Membrane cost can reach over 60% of the material cost when large scale applications are considered [5]. Therefore, to promote the development and implementation of this technology, both economic and technical optimization of these components become essential, as well as improve their service life, since a material with a stable long-term behavior is more convenient from an economic point of view.

When the specific electrode reactions are concerned, oxygen reduction reaction (ORR), with its slow kinetics and high overpotentials, often represents the limiting step of the whole process, so that the synthesis of suitable cathodes has a crucial role [6][7][8]. Cathodes are usually composed of two components: the support (working as current collector) and the catalyst. Carbonaceous materials have been extensively used for both cathode and anode supports in MFC applications [9] [10]. In the case of the cathode, several materials have been used: carbon felt (CF) [11], veil [3], cloth (CC) [8], mesh (CM) [12], etc. However, very few studies compare the different materials, to identify the most cost-effective one. One of the most remarkable is the work of Santoro et al. [9] in which carbon cloth, veil and mesh materials were tested as cathode support and electrode, on a C-MFC. They found a linear relationship between morphological parameters at nanoscale and current produced, probably due to an improvement of the cathode-separator contact. CM proved to be the most cost-effective material when microporous layer and Pt-free catalyst were added.

One of the reason why traditional MFCs struggle for wide range deployment is that platinum is used as the ORR catalyst [8]. However, as discussed in the literature [10] [13], Pt rapidly decreases in catalytic activity when working in MFC (deactivation rates of more than 50% after 4.5 months have been reported [14]), mainly due to its propensity for surface poisoning and biofouling. This fast deactivation, coupled with its high cost, makes Pt suitable only for

laboratory studies under ideal or clean conditions [13]. Therefore, it is of high importance to find a non-expensive electrocatalyst with high ORR activity in the given temperature range.

Biological and inorganic catalysts have been investigated as alternative to Pt. Enzymes and bacteria have reported interesting results [15][16], but they have also shown rapid denaturalization and deactivation [16]. Among other inorganic catalysts (such as Pt group metals or metal-free carbon-based materials), transition metal oxides like FeO [17], CoO_x [18], etc., have been often proposed as catalysts for ORR, because of their low-cost, environmental friendliness, high ORR catalytic activity and, especially, abundant availability [19][20]. A recent study [18] investigated the effect of Co_3O_4 and Fe_3O_4 catalysts on conductive ink printed cathode, with carbon felt support: the cathodes exhibited a comparable performance (6.62 $W \cdot m^{-3}$), even significantly superior to Pt, confirming that transition metal oxides are real cost-effective substitutes to Pt.

Recently, copper oxide has drawn extensive attention because, in addition to the common characteristics of transition metal oxides, it possesses also anti-fouling properties [21][22][23], a crucial parameter for MFCs long-term performance. However, in spite these optimal properties, only few studies have examined the use of copper oxides as catalyst in MFCs. Zhang et al. [24] prepared N-type Cu_2O doped activated carbon by electrodeposition and analyzed its performance as cathode catalyst. The obtained power density (1390 ± 76 $mW \cdot m^{-2}$) was almost 60% higher than control cathode (AC bare). This group also evaluated the impact of morphology and micro-structure of copper oxides by adding different kinds of surfactants in the electrodeposition process [22]. They found that CuO deposits with high amount of holes or iso-oriented mosaic structures enhanced the ORR catalytic activity. Yang et al. prepared hydrangea-like Cu_2O@N-doped activated carbon cathodes [25], with a great catalytic activity of ORR (1610 ± 30 $mW \cdot m^{-2}$) due to hydrangea-like structure and simultaneous carbon N-doping. The influence of electrodeposition time was also studied [26], and a maximum power density of 308.69 $mW \cdot m^{-2}$ was obtained for a moderate value of 100s; longer deposition times resulted in a decrease of the specific surface area, thus reducing the electrocatalytic activity of the cathode. In addition, copper oxides have been also tested as photocathode in MFC due to their excellent photoconductive and photochemical properties [27].

It is worth mentioning that most of the studies dealing with Cu_xO-based catalyst refer to MFC separator-less configuration. This option is characterized by a low complexity of

design, reduction of material costs [28], as well as high power outputs due to low internal resistance [29]. However, by removing the separator, diffusion of oxygen from cathode to anode side occurs, resulting in loss of substrate and drop of coulombic efficiency [10]. Furthermore, in the absence of a physical barrier, cathode tends to foul rapidly, by formation of aerobic bacterial biofilm (biofouling) on the catalyst surface, which increases the internal resistance, thus affecting the system performance [30]. Therefore, this configuration is not recommended for long-term operation, and thus for industrial applications.

As far as separator is concerned, Nafion is the most widespread option for proton exchange membranes in low temperature (≈200 °C) fuel cells [31] [32]. It is characterized not only by a high ionic conductivity, but also by its high cost and low lifetime in high organic load media [33]. Therefore, Nafion membrane is considered as unsuitable for scaling up purposes [28] [34]. More than 20 different alternatives have been proposed in literature [35][32], such as AMI 7001, cloth separators, agar membranes, etc.

Among all of them, ceramic materials have emerged strongly in recent years [36] due to their great natural availability and low-cost: when used as MFC separators, they present good chemical and thermal stabilities, relatively high mechanical robustness, simple washing, not-ion selectivity, etc. [37]. Several studies revealed the crucial effect of physical and chemical parameters, strictly connected to the manufacturing procedure [38][39], such as composition, thickness, porosity, pore size distribution, that can affect the flux of ions through the separator, and in turn the MFC performance. As an example, the sintering temperature of ceramic membranes was of paramount importance in determining its final porosity and pore size distribution [34]: high sintering temperatures dramatically reduces the fine porosity fraction of the membrane and favors the formation of large but closed voids (pore coarsening effect). On the contrary, lowering the sintering temperature from 1410 °C to 1030 °C, leads to an improvement of the MFC power output by almost 60 %, thanks to the higher volumetric proportion of fine pore in the microstructure, which entails a lower membrane resistance.

The influence of ceramic membrane thickness on the performance of MFC have been explored by different works [40][41][42]. In all of them, being the ceramic material the same, thinner ceramic membranes outperformed the thicker ones, 2 mm being the lowest thickness value studied up to the date. However, in a recent study, the authors estimated an optimal theoretical thickness of 1.55 mm for planar same composition (terracotta) membranes [43]. In addition, the effect of the membrane thickness can vary when different ceramic (solid

oxide) based materials are considered [40]. Among the different kinds, suitable for MFC membrane application, terracotta, earthenware, mullite, alumina, pyrophyllite, etc. [38,40], have been considered as well as mixtures and composites [44][45]. In all cases a great influence of the ceramic composition over the MFC performance was observed.

It may be also considered that, with a suitable design, ceramic separators or membranes can play a dual role: medium for ion exchange and MFC chassis. Compared to planar design, tubular or cylindrical configuration has become the most popular choice because of: their efficient use of space, potential scaling up, commercial availability in stores, versatility to work with mix and continuous liquid flow, real-world applications demonstrated, better membrane-electrode assembly, added-value catholyte synthesis and storage, etc. [46].

Therefore, the development of ceramic membranes strongly depends on finding the optimal combination of physical-chemical properties and architectural design. However, this contrasts with the fact that most of the authors working on C-MFC use commercial products like pots [47][48] or acquire their ceramic membranes from different providers [49], whose properties cannot be, usually, custom-modified (in terms of porosity, diameter, thickness, composition, etc) at lab scale [50]. In order to achieve the above goal, different researchers claimed the need of a rigorous ceramic processing procedure which allows modification and evaluation of ceramic membranes in a precise, simple and economical way [37,51]. A good candidate for such technology is a simple slip-casting technique. Slip-casting is a mature, cost-effective, and simple almost near-net shape methodology which has been traditionally used in ceramic processing for centuries [52]. Besides its simplicity, this technique enables accurate control of the microstructure, this allowing the preparation of good quality, thin wall products with a possibility for certain complexity in shapes [53]. The slip-casting has been increasingly used for advanced technical ceramic applications (especially in tubular shape) where rigorous control of properties is a must, such as: tubular and microtubular solid oxide fuel cells [54] [53], drinking and wastewater treatment [55], gas separation [56], etc. To the best of our knowledge, this technique has never been used to manufacture customized ceramic membrane separators for MFC; it can meet the requirements of repeatability, accuracy and simplicity demanded by the scientific community working on C-MFCs. In addition, slip-casting is a well-stablished technique widely employed in the ceramic industry, which would greatly facilitate the industrial production of ceramic membranes.

The low-cost systems reported in literature are usually focused on the optimization of one component of the MFC, and the cost analysis, when presented, is limited to this single modification. However, considering all the above, in order to reduce the cost of MFCs not only cheap materials should be introduced, but also low-cost processing and manufacturing techniques should be deployed. For these reasons, the present work was aimed to combine inexpensive materials with economic, simple and efficient manufacturing technique as a strategy to optimize the most critical components of MFC: separator and cathode. A new cost-effective Ceramic-MFC cell has been designed, built, and completely characterized; slip-casting has been successfully validated for the first time as a methodology for manufacturing tubular ceramic membranes for MFC. The accuracy of this technique has been tested by fabricating tubular ceramic separators with a thickness of 1.5 mm, the lowest, to date for this type of separators, according to the theoretical optimal value indicated in literature [43]. Regarding the cathode, different carbonaceous materials have been studied, identifying the one with the best performance/cost ratio. Carbon Mesh (CM) has been used to deposit a low-cost commercial CuO-based catalyst, by means of a simple, widely used and economical spraying technique. As far as our knowledge goes, this is the first time this methodology is used with CuO based catalyst for ceramic membranes. In addition, a rough economic analysis of the manufacturing cost of the presented cell has been made, including aspects such as energy consumption.

2. Experimental

2.1 The Experimental set-up

Single chamber air-cathode Microbial Fuel Cells with a tubular ceramic membrane were used in this study. The C-MFCs had a two-compartments cylindrical configuration, divided by the ceramic membrane: the external cylinder constituted the anode, where biofilm was grown, while the internal cylinder was the cathode, which was in direct contact with air. Thin titanium wires were used to sew the planar electrodes in the cylindrical shape, as well as to guarantee the electrical contacts. Typical polypropylene lab jars were used as holder for the electrodes-membrane assembly. The total volume of the anodic solution was 150 mL. Suitable openings were provided on top of the chambers, to fill and drain the anodic compartment. Figure S1 (Supplementary Documentation) shows a representation of the C-FMC configuration used in the present study.

2.2 Membrane fabrication by Slip-Casting

One of the novelties of this work involves the fabrication of the end-closed cylindrical ceramic membranes by a simple and inexpensive slip-casting technique based on the following procedure: firstly, suspension of clay (Pastart, Argiles Bisbal SL) was prepared by adding the as-received clay to distilled water (300 $g \cdot L^{-1}$). Then the suspension was homogenized with high torque stirrer for 2 h at room temperature. The obtained stable clay suspension was poured into the plaster molds and kept for a defined period of time, to allow the formation of thin clay coating due to capillary action of plaster mold. The remaining suspension (excess) was then poured out, and the deposited clay was left for drying during 24 hours within plaster mold. De-molded membranes were sintered by performing a thermal treatment step at 950ºC with a dwell time of 2 h.

Microstructural and morphological characterization of obtained ceramic membranes and electrodes was done by performing Scanning Electron Microscopy (SEM) analysis with Jeol JSM 6010 Microscope (JEOL, Ltd, Tokyo, Japan) with integrated Electron Diffraction Scattering (EDS) probe.

The water saturation method was used to measure the porosity of ceramic membranes [57] (as reported in Standard UNI EN 1936:2007). The thickness of the ceramic membrane samples was measured by a Digital Caliper (Mitutoyo 500-196-30 Absolute), taking an average thickness value of 5 measurements. Thickness dimensions were also confirmed by measuring the cross-sectional SEM images.

To the best of our knowledge, there is no optimal or preferred porosity or thickness values for ceramic membranes in MFCs applications, as they are related properties which also depend on multiple factors: composition, pore size distribution, tortuosity, etc. Regarding porosity, membranes with porosities ranging from 2% to more than 30 % can be found in C-MFC studies [58]. In our case, a value of 20-30% was estimated when clay suspension was prepared. This is a medium-high range of usually reported values, but quite common in works where ceramic separator contribution was evaluated [50] [50] [81].

Regarding the thickness, as discussed in section 1, several studies have shown that thickness reduction leads to improved performance of C-MFCs [42]. However, to the best of our knowledge no study has reported tubular or cylindrical ceramic membranes with thickness lower than 2 mm, ranging normally from 2 to 18 mm [37,58]. In order to demonstrate the capacity of slip-casting to manufacture ceramic membranes with defined geometries and properties, a value of thickness of 1.5 mm was selected.

It is important to point out that in this study, we sought to validate the use of slip-casting to manufacture ceramic membranes for C-MFCs. For this reason, the variation in the properties of the manufactured membranes has not been studied in depth, and values similar to those reported in the literature have been used. Of course, the porosity and thickness effects and the identification of their optimal values could be the subject of a specific study, but this is not the aim of the present work.

2.3 The Electrodes

During inoculation of the C-MFC (biofilm formation process), 2.5 mm thick carbon felt was used for anode and cathode. However, once the cell was matured and the electrical response was stable, the following carbon-based materials were tested as cathode: carbon cloth (CC), carbon mesh (CM) and carbon felt (CF) with thickness of either 2.5 mm (CF2.5), or 5 mm (CF5). Those materials were respectively supplied by Zoltek Corp. (Hungary), SGL Carbon Group (Germany), and SCHUNK GmbH & Co. KG (Germany). Before testing, all materials were pre-treated by immersion in acetone for 24 h to remove impurities. Then they were washed with distilled water and dried in air atmosphere at 150 ºC for 2h. To ensure all samples had the same operation conditions and starting point, CF2.5 cathode used during inoculation was replaced by a new sample for the evaluation of this material.

After carbonaceous materials were characterized, catalytic layers were coated on the best cost-effective performing one, using a commercial low-cost CuO-based catalyst (kindly supplied by Sotacarbo S.p.A) containing around 60 wt.% of CuO along with other different metal oxides. Powder of catalyst was obtained from the original pellets, by 2 h ball milling pre-treatment. The obtained powder was used to prepare an ink, following a procedure indicated in the literature [59]: 120 mg of catalyst and 120 mg of carbon black were mixed with 0.8 mL of Nafion (Thermo Fisher Scientific Inc.) and 20 mL isopropanol, and sonicated for 2 h. The ink was sprayed on the support up to a load of 3.5 mg catalyst $\cdot cm^{-2}$. This catalyst loading is in the range of common reported values for nonprecious metal catalysts for MFC cathodes [60]. The final cathode was thermally treated at 100 °C for 1 h, to remove the solvent, and left at room temperature during night to consolidate.

Also, for comparison, a specific cathode with a load of 0.5 mg $Pt \cdot cm^{-2}$ was prepared, following the same procedure adopted for CuO-based cathodes. In this case, Pt/C powder (60 wt.%, Alfa Aesar, Thermo Fisher Scientific Inc.) was used.

As for ceramic membranes, structural and morphological properties of different cathodes were studied by Scanning Electron Microscopy (SEM).

2.4. Inoculation

The cell operated at 23-25 °C, at neutral pH. Sewage sludge from the anaerobic digester of the Ciudad Real (Spain) wastewater treatment plant was used to inoculate the MFCs. Inoculation was performed by filling the anodic chamber with 150 mL of solution, in which 50% of sedimented sludge was mixed with 49% of medium (80 $g \cdot L^{-1}$ K_2HPO_4, 13 $g \cdot L^{-1}$ KH_2PO_4, 1.3 $g \cdot L^{-1}$ NH_4Cl, 26 $mg \cdot L^{-1}$ $FeCl_2$; 5 ml of mineral media [61]) and 1% of sodium acetate (200 $g \cdot L^{-1}$). Before inoculation, nitrogen was sparged continuously for 20 min to maintain anaerobic conditions in the anodic chamber. During the biofilm growth, a 150 Ω external resistor was connected to the C-MFCs. The growing process of the biofilm was checked by monitoring the trend of potential with a data acquisition system, consisting of a 32-bit data acquisition card (782604-01, NI, USA) and a custom-made software developed with LabView 2015 (NI, USA).

Two inoculation steps, with a duration of 7 days, were performed to promote the biofilm growth. After that, inoculum was removed, and only the medium with acetate was fed to the cell. Three cycles *substrate addition-depletion*, with similar potential response, were generally considered sufficient to stabilize the biofilm. Afterwards, the anolyte was replaced when the potential dropped below 10 mV.

SEM analyses were also used to confirm the presence of the biofilm on the electrode surface. Before SEM, biofilm samples were fixed, rinsed, dehydrated and gold coated following a conventional procedure [62].

To investigate the diversity of bacterial community, biofilm was subjected to pyrosequencing analysis. DNA was extracted with the Biofilm DNA Isolation kit ® (Norgen Biotek Corp.), following the manufacturer's instructions. The samples were sent to an external laboratory for pyrosequencing.

2.4 Electrochemical characterization of the cells

Polarization curves (PCs), cyclic voltammetries (CVs) and linear sweep voltammetries (LSVs) have been used to characterize the cells from an electrochemical point of view. In particular, a variable resistor box (R_{ext} from 20 Ω to 470 kΩ) was placed between the power supply and the cell, and the voltage drop (V) across the resistor was monitored. A stable

potential value was measured after 10-15 minutes approximately. The power generated by the system was calculated as P=VI: the current (I) was obtained from the measured voltage, based on Ohm's law as $I = V/R_{ext}$. The open circuit voltage (OCV) was also measured. The polarization curves (I vs V) obtained for each MFC, allowed the internal ohmic resistance to be determined, from the slope of the linear trend.

CVs and LSVs were performed with an electrochemical workstation (VMP-3 Bio-Logic Science Instruments). LSVs were carried out in a specific three-electrode cell, in which a Pt grid and the carbon material were used as counter and working electrode, respectively, being Ag/AgCl (E_0= 197 mV *vs* NHE) the reference electrode. During LSVs the cell potential was scanned at 0.2 $mV \cdot s^{-1}$, while electrolyte was constituted by the medium solution at pH 7.

In the case of CVs, bioanode and cathode served as working and counter electrodes, respectively. CVs were carried out at scan rate of 1 $mV \cdot s^{-1}$ within a potential range of −0.6 V to +0.3 V (Vs Ag/AgCl), at different biofilm growth stages, and under different electric activity of the biofilm: the two conditions of *turnover* and *non-turnover* were also investigated, in the presence and in absence of acetate, respectively. Analysing the results obtained from these two different conditions, valuable information about the electron transfer processes can be achieved, such as: redox species involved, the bioelectrocatalytic activity of the bioanode, influence of the mass transfer, etc.[63][64][65]. Non-turnover conditions were achieved starving the biofilm overnight in acetate-free medium, to deplete acetate, possibly absorbed into biofilm surfaces or within bacterial cells. CV measurements allowed deriving information on the extracellular electron transfer mechanism of the biofilm.

2.6 Coulombic efficiency - The bioelectrochemical performance of the C-MFCs, was also monitored by evaluating the Coulombic efficiency (CE) (eq.1), based on the total charge measured and the related change in chemical oxygen demand (COD), over one cycle [44]:

$$CE = \frac{M \int_0^t I dt}{nVF(COD_0 - COD_t)} \qquad 1)$$

Where:

- *M:* molecular weight of O_2;
- *I:* generated current;
- *t:* time duration of the cycle;
- *n:* number of electrons exchanged;

- *V:* anodic compartment volume;
- *F:* Faraday constant;
- $COD_0 - COD_t$: change in chemical oxygen demand (COD) over the time of operation (t).

3. Results and discussion

3.1 Morphological characterization of Clay Ceramic Membranes fabricated by Slip-casting

The capacity of the slip-casting was evaluated to manufacture membranes with different properties: porosity, geometry, composition, thickness, etc. Figure S2 (Supplementary Documentation) shows the SEM cross-section images of tubular membranes of different thicknesses. In Figure S3, images of membranes manufactured by slip-casting with different geometries and materials are also presented. In addition, Figure S3 g) shows the characterization of two membranes with different geometry, but almost identical thickness and porosity values.

As stated above, 1.55 mm was considered as reference value for MFC separators fabricated by slip casting. In fact, thickness of 1.5 ± 0.32 mm was measured for these separators by the digital caliper. The separator thickness was also measured by the cross-sectional SEM images (Figure 1 A), confirming the obtained value.

An average porosity around 26% was calculated by water absorption method. Although it can be considered a medium-high porosity, it is in good agreement with the results of recent C-MFCs works [34,50,66]. For instance, You et al. [50], obtained porosities between 22-27% for custom made separators using a cylindrical shape.

Regarding the microstructure, higher magnification cross-section SEM images (Figure 1b) confirmed a microporous structure, with flake-shaped particles of irregular dimensions. Pores were widely distributed in the sample; a non-homogenous size distribution was observed with variable diameters ($\leq$ 10 μm), which well agrees with that described in literature for clay separators [38][44].

EDS spectrum of membrane is reported in Fig. 1 c), along with the chemical composition (inset), which was estimated from the stoichiometric ratio of each individual element. Analogous soil-based materials were used in literature [38] [5], such as earthenware, terracotta, etc., characterized by a predominant presence of SiO_2, which, according with

some of these authors, could improve ionic conductivity and hygroscopic properties, thus favoring a better performance of the membranes. In fact, Pasternak et alt. [38] studied the performance of different ceramic materials as MFC separators, and they found that best performances corresponded to separators with higher amounts of SiO_2: earthenware (67.92%) and pyrophyllite (64.54%). These percentages are quite similar to that obtained for our separators (64.66%).

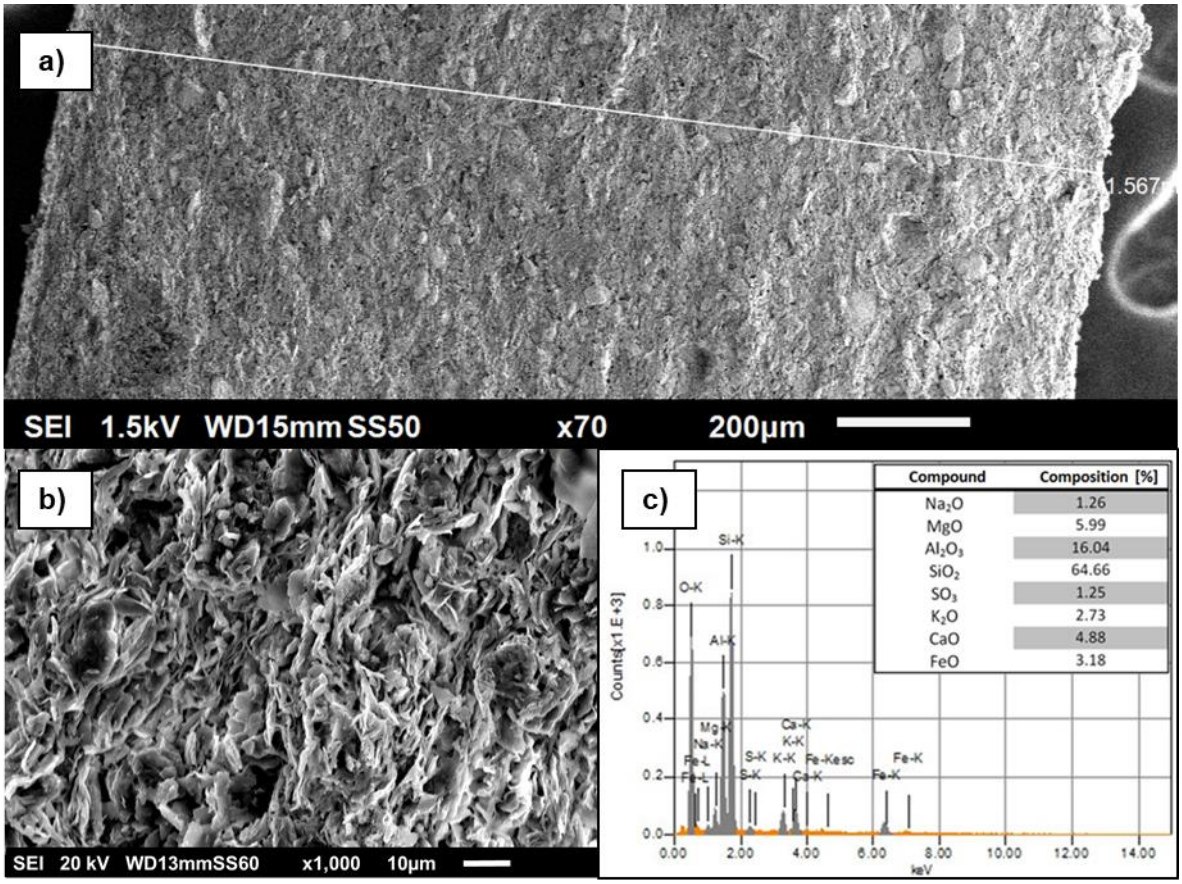

Fig.1.: SEM micrographs correspoding to fracture cross section of clay slip-casted membrane: a) general view indicating 1,5 mm thickness, b) close up at the microstrutural features and c) EDS spectra correspoding to the area of the micrograh b.

The obtained results confirmed the versatility offered by this fabrication process to get membranes with customisable charactersitcs in a simple and economic way. In addition, the potential scaling up of slip-casting was also verified by the fabrication of ceramic separators with different shapes, but maintaining the same structural properties (porosity and thickness).

3.2 Inoculation stage and electrochemical characterization of the Ceramic-Microbial Fuel Cell

During this stage, the enrichment of electrogenic bacteria in the anodic compartment is sought, and more specifically the formation and maturation of a biofilm on the anode surface.

Figure 2 shows an example of the trend of the potential recorded for C-MFCs. After a lag phase of approximately 2 days, it is observed a gradual increase in electrical response. This initial response is due to first stage of biofilm growth, and then it reaches a stable phase characterized by a higher potential. After the first week, the potential gradually decreased with the carbon source concentration. However, when the second inoculation cycle started the potential quickly regained a stable value, very similar to the previous one. The observed trend is quite similar to that reported by Paternak et al [38]. They obtained lag periods of 2-3 days and reached the maximum power performance after 5 days of operation, which is in well agreement with our results. These authors also observed a potential decrease during the first day, before reaching the stable high electrical response. This behavior is related to inoculation methodology. Paternak et al [38], completely removed the inoculum from the reactor during the activation stage. This entails the elimination of planktonic bacteria and electron shuttles, widely present in activated sludge [67]. However, in the present work, the sludge is always present during the maturation stage, and thus a relevant contribution of these kind of bacteria and electron mediators can be expected.

After two weeks, it could be considered that the microbial biofilm was matured and formed over the anode surface. This is confirmed by the SEM images (Figure 2 inlet), which provide direct visual information about the biofilm grown on the anode surface fibres. As can be seen, before the maturing process, a carbon felt fibre surface is smooth, with a regular morphology. However, when the biofilm was formed, there is a significant presence of bacteria attached to the surface of the fiber, constituting substantially a heterogeneous layer which covered the fibre unequally. However, the microbial biofilm has not finished growing, and it will continue over time. Although this trend can initially improve the electrical response, some authors have pointed out [68] than long-term operation should result in thicker biofilm which could cause mass transfer limitations within the biofilm and, ultimately, a decrease in power production.

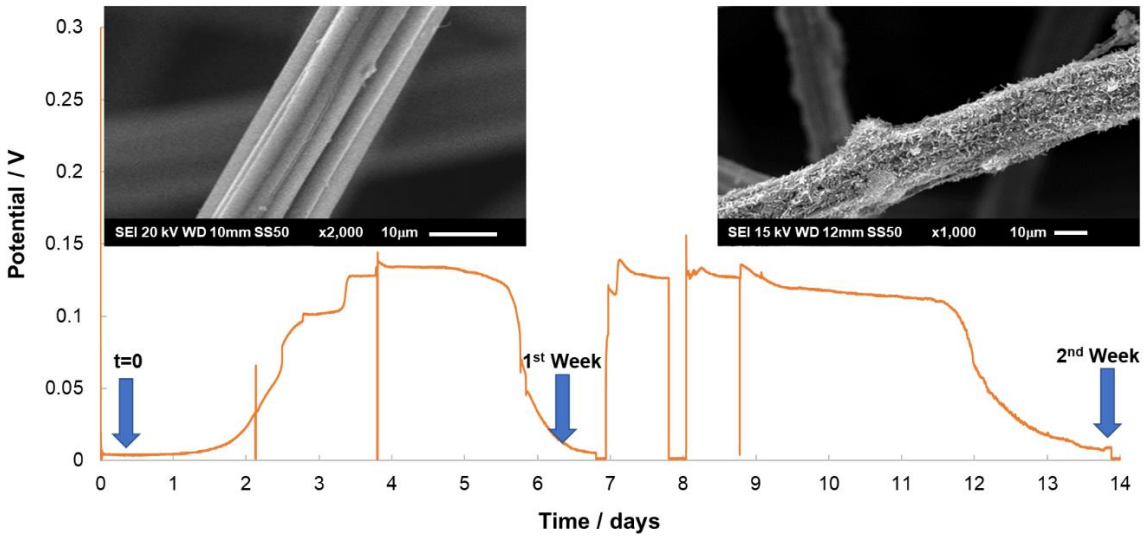

Fig.2. Example of trend of potential with time, measured during the first 2 weeks. Inset: SEM micrographs of the substrate support before and after the biofilm growth.

Information on charge transfer between biofilm and substrate were derived by cyclic voltammetries in conditions of *turnover* and *non-turnover*. In order to monitor the activity of biofilm at different stages of growth, CVs were carried out weekly.

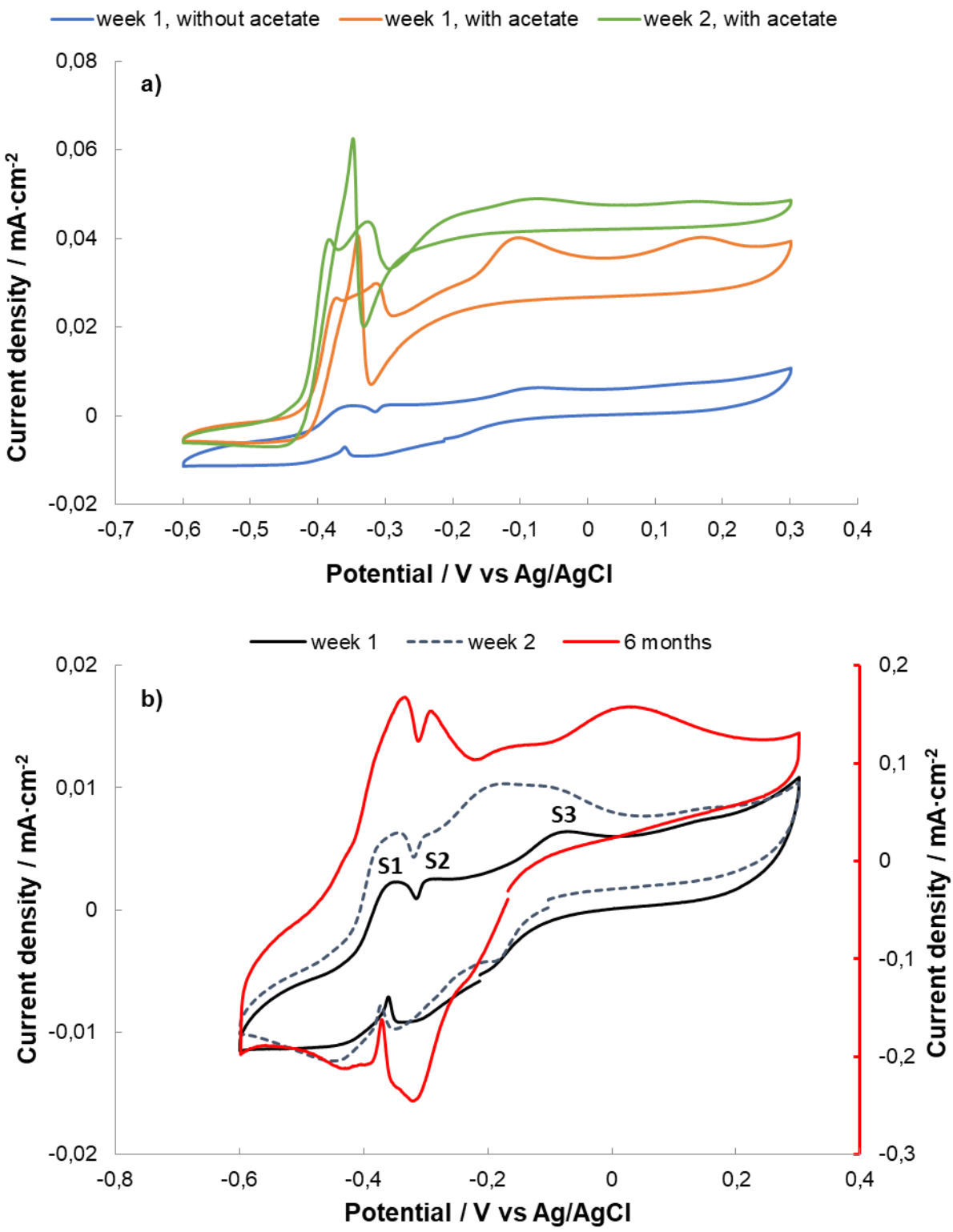

Fig.3. Cyclic voltammetries for slip-casted Ceramic-MFCs at different biofilm formation stages: a) comparison between non-turnover and turnover conditions; b) comparison between differently aged biofilm in non-turnover conditions: 1 week and 2 weeks aged biofilms and at 6 months aged biofilms (red curve, secondary axis).

An example of CV is reported in Figure 3. In *turnover conditions* higher anodic currents are measured, thanks to the enzyme kinetics. Actually, when the solution contains an excess of acetate, which acts as electron donor, the current measured at the bioanode is the result of a continuous reduction of the active sites by the microbial metabolism, which occurs in series with the subsequent oxidation by the electrode. However, while the electrochemical reaction depends on the potential, the biological reduction rate can be considered as independent of potential and of the other electrode parameters: it only depends on the number of microbial cells, and their activity in the biofilm as wells as the respective substrate concentrations. Under ideal conditions, this rate can be described by Monod and Michaelis–Menten kinetics, and an S-shape curve is obtained: no reduction peak is observed in the voltammogram and, if the scan rate is slow enough, the maximum current is only dependent on the enzyme kinetics, or on the mass transfer [64].

In the present case, a quite irregular S-shape of CV is obtained (Fig. 3 a) from cell where biofilm was newly formed: an additional oxidation peak is well visible also in the reverse scan at a potential value of about -0.4 V, while no reduction peaks appear at relevant extent in the reverse scan. Moreover, increase of the bioelectrochemical activity with time is well visible: after 2 weeks the current in the CV, and then the bioelectrochemical activity of bacteria, increases, possibly due to an increased biofilm coverage of the surface. The increasing amount of electroactive bacteria attached to the anode surface improved the kinetics of the bioelectrochemical reactions [68].

The effective proliferation of the biofilm electrochemically active was generally assessed by SEM analyses (see Fig.2 inset), performed at a sample at the end of the service life of the electrodes.

CVs obtained under *non-turnover* conditions are compared in Figure 3b): in this case the electron source given by the substrate is missed, so that the exchange of charge is the result of the electroactivity of the biofilm already present at the electrode surface. The height of the related voltammetric peaks, may be an indication of the biofilm growth in time: the higher bacterial density, the higher concentration of metabolites in solution, which in turn, influences conductivity and capacity. The potential of the peaks is instead connected to the redox species, i.e. to the specific class of bacteria present in the biofilm. The formal potential (E_f), evaluated as average value between the two potentials of the redox couple, is generally assumed to characterize the bacterial species. Thus, for example, three major systems (S1 to

S3) are individuated with formal potential (E_f) and potential peak distance (ΔV) reported in Table 1, which may represent the species mainly responsible for the charge transfer of the biofilm newly formed. The presence of the *Geobacter* could be indicated as corresponding to the formal potential of systems S1 and S2 which are in the range generally reported in literature for this bacterial species (-0.2 V and -0.4 V vs Ag/AgCl [64]).

The presence of electrogenic bacteria was confirmed by pyrosequencing analysis. Phylum and genus distributions are shown in Figure S4. From these results, firstly, the presence of Geobacter bacteria is confirmed, albeit in a small proportion. Moreover, several genera with electroactive members have also been identified, such as: Desulfuramonas [69], Pseudomonas [70], Costridium [71], etc. Although the genus Desulfuramonas emerges as the most abundant in the biofilm (12%), the bioelectroactive response is assumed to be the result of a synergistic mixed-culture biofilm community, in which different species perform specific functions [70].

Table 1. Values of the formal potential E_f and potential distances of the redox peaks individuated in the CV recorded during the first two weeks of biofilm ageing

	1 week		**2 weeks**	
	E_f / mV	ΔV / mV	E_f / mV	ΔV / mV
S1	-375	90	-380	100
S2	-265	150	-305	30
S3	-130	100	-195	90

It is expected that long-term operation should result in a thicker and more matured biofilm as discussed before. In this case, the peaks should become more clearly distinguishable, indicating an increment of the bioelectrochemical response and, probably a better bacteria colonization. For comparison, in Figure 3b, CV of a long-term operation (6 months) C-MFC is also shown.

In fact, comparing with the first two weeks response, an appreciable improvement in the bioelectrochemical activity is observed for the long-term C-MFC, where current peaks increase of more than one order of magnitude (red curve in Fig. 3 b is reported in different

y-axis, for a better comparison). Moreover, as assessed by the potential of the peaks, in both cases the most important bacterial activity is revealed in the range between -0.4 V and -0.1 V. As the biofilm stabilizes, peaks tend to shift towards more negative potentials, indicating a better electrocatalytic activity, and the distance between oxidation and reduction potentials related to S2 decreases, which indicates a more reversible process. However, the comparison with the curves obtained in *turnover* conditions (Figure 3a) reveals that, as the age of the biofilm increases, the redox processes S1 and S2 are mainly the responsible for the electron transfer, whereas systems S3 appears less electrocatalytically active.

3.3 Performance with different cathodic materials

Morphology of different carbon-based cathodic materials was studied by SEM. In Figure 4, dense texture of fibers is observed at CC, while the weaving of the fibers in the CM is wider and tidier. Finally, the fibers in CF appear massively disordered and three-dimensionally distributed. The average diameter of the fibers was 8, 7 and 15 ± 2 μm, for CC, CM, and CF, respectively.

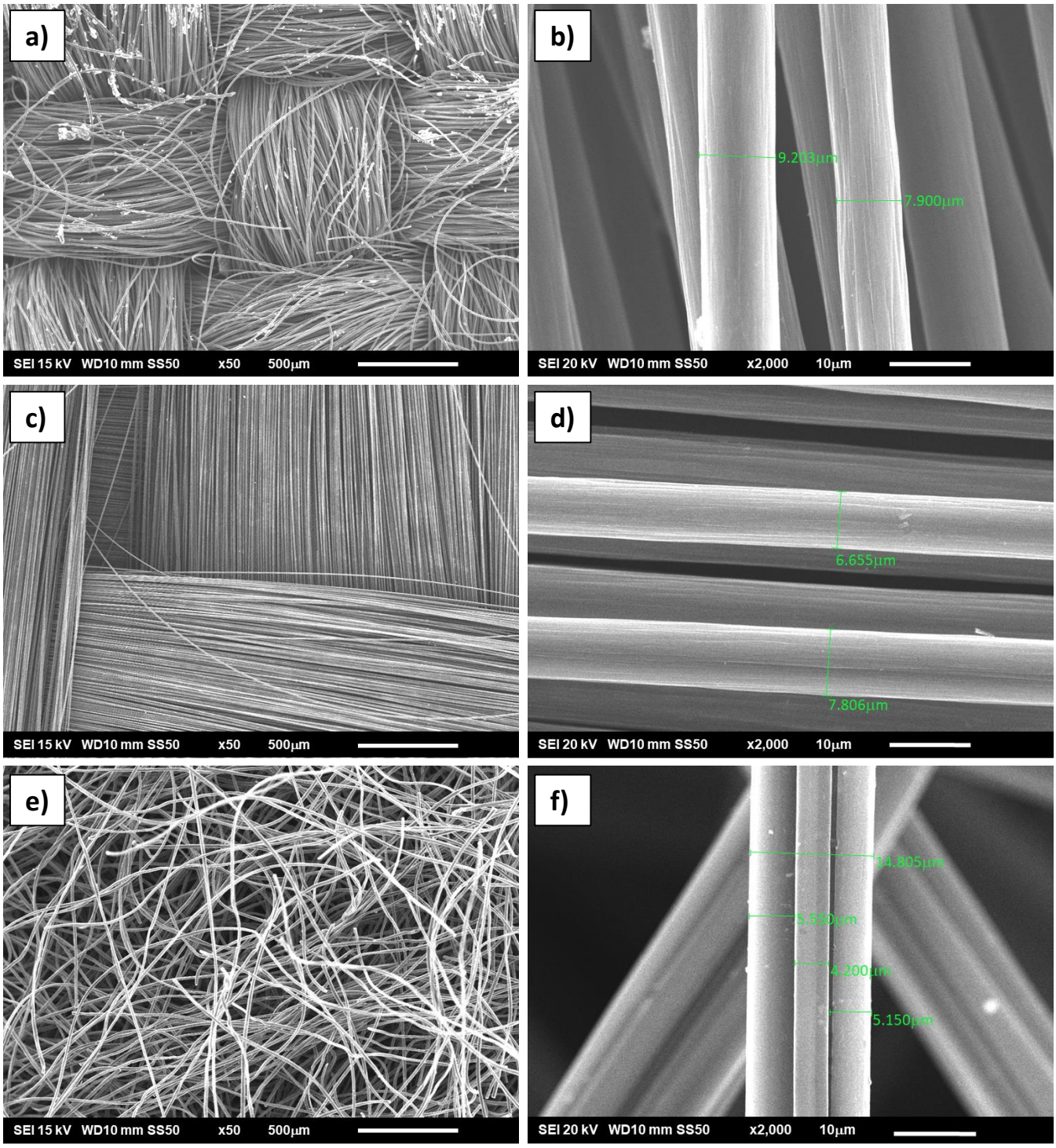

Fig.4. SEM micrographs of the different supports: CC (a, b), CM (c. d), CF (e, f). Left and right columns correspond to X50 and X2000 magnification, respectively.

Regarding electrochemical characterization, LSV were firstly performed on each cathodic material, being a Pt grid used as anode (see section 2), to avoid the anodic processes became limiting: in this way, possible limits of the cathodic ORR could be instead evidenced.

The results have been elaborated in terms of logarithm of the current density versus overpotential, evaluated with respect to the oxygen redox potential in neutral solution, and considering the Ag/AgCl reference electrode potential. Kinetic parameters reported in Table 2 were derived by the Tafel analysis. Values of *b* around 60 $mV \cdot dec^{-1}$ are derived for all the investigated materials. A wider variability of i_o values was obtained, with values ranging in the order from 10^{-10} $mA \cdot cm^{-2}$ to 10^{-8} $mA \cdot cm^{-2}$, indicating an activity of the samples in the order: CC<CF5<CM<CF2.5. Slope and current density values are quite consistent with that obtained by other authors for non-catalyzed carbon cathodes [72] [73] [74].

Table 2. Tafel parameters calculated for the different cathodic materials.

Cathode	**b ($mV \cdot dec^{-1}$)**	**i_o ($mA \cdot cm^{-2}$)**
CC	55	2.54×10^{-10}
CM	60	8.04×10^{-9}
CF2.5	71	1.22×10^{-8}
CF5	63	3.09×10^{-9}

The carbon materials were then used as cathodes in C-MFCs (operated for two months) where a stable biofilm was formed at the anode: the performance of the cells was monitored in terms of potential values originated across an external load (150 Ω), selected from the resistor box.

Depending on the cathodic material, different maximum potential values were measured at the cell. Data were confirmed by three repeated cycles. Table 3 resumes the average values and standard deviation of maximum potential measured and the related current obtained in the different conditions.

The best electrical response corresponded to CM, followed by the thicker CF. However, given the small difference between both average potential values and the magnitude of the standard deviation for each of these measurements, these values can be considered almost equivalent. CF2.5 reported a current value very close to the previous cathodes. Finally, it is remarkable the low electrochemical response when C-MFC worked with the CC cathode, becoming almost half of the other three materials. This result was surprising and unexpected

for two reasons. First, CC is usually the reference material for the construction of air-cathodes in single-chamber MFCs and it had been widely used [8,14]. Second, this material had previously shown the best performance when compared to other carbonaceous materials for MFCs [9].

Table 3. Average values (3-fold repeated runs) and standard deviation of maximum potential measured, and the related current obtained for each cathode.

Cathodic Material	**V_{max}(mV)**	**SD**	**I_{max} (mA)**	**SD**
CC	30.9	±9.8	0.206	±0.065
CF2.5	54.4	±2.1	0.363	±0.01
CF5	57.4	±2.6	0.383	±0.02
CM	58.8	±6.4	0.392	±0.04

The previously described procedure, repeated for the different R_{ext}, for small periods of time, allowed the polarization curves and the related power curves to be obtained. Figure 5 shows the comparison from the polarization experiments carried out from the four carbonaceous materials.

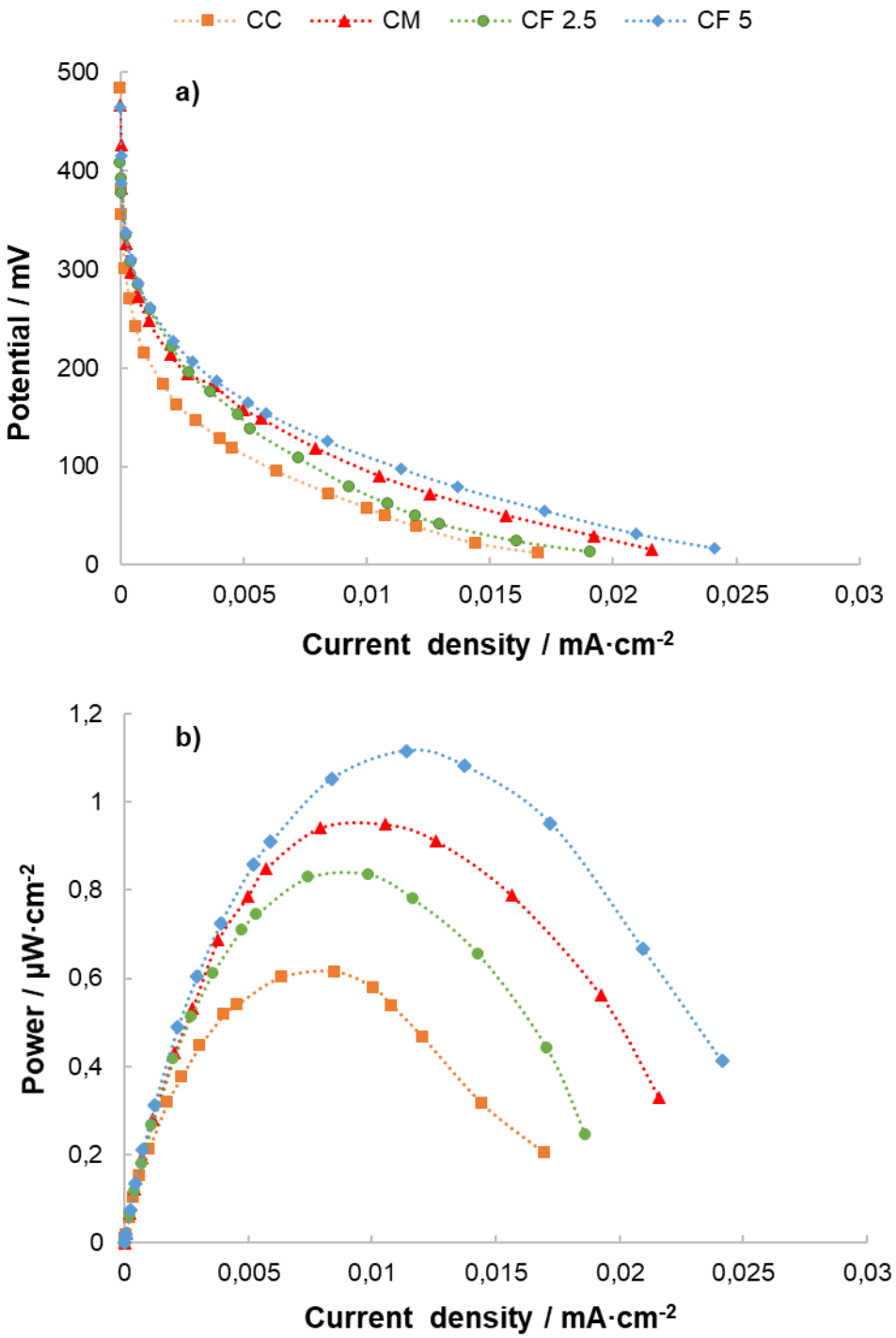

Fig.5. Examples of polarization (a) and power curves (b) of the MFCs in which the different materials were used as cathode.

The obtained polarization curves showed the shape typically reported in literature [15]: an initial non-linear change in potential was always observed, due to activation losses at low

current densities, followed by a linear range, over most of the useful range of current densities, indicating that all the examined systems operate at current densities where ohmic losses are dominant. Of note, since in all the cases the anode material was always the same, differences in the trends could be attributed to the different performances of the cathodes.

Polarization data have been used to estimate the value of the internal resistance (R_{int}) of the cell by the electrode potential slope method [75]: values of R_{int} were obtained from the slope of the linear portions of the polarization curves, while the activation losses were calculated as the difference between the experimental open circuit potentials and the y intercepts of the linear trend line. Table 4 resumes the main parameters derived from the analysis of polarization data. Data of coulombic efficiency (CE %) are also reported to complete the comparison.

Table 4. Analysis of the polarization data for the MFC equipped with different cathodic materials.

		CF2.5	**CF5**	**CM**	**CC**
Polarization data	**I ($mA \cdot m^{-2}$) measured at 50 mV**	120	172	156	107
	OCV (mV)	422	425	471	484
	R_{int} (Ohm)	344	334	278	280
	Activation overpotential (mV)	174	211	225	260
	Max Power density ($mW \cdot m^{-2}$)	8.1	11.2	9.5	6.2
	CE %	13.29	16.55	11.47	10.69

If data are considered in terms of both the OCV and the R_{int} values, two different trends are identified at CF electrodes, and CM and the CC ones. In the case of the OCV, when the cell worked with CF electrodes, the OCV value was approximately 10-13% lower than that when CM or CC were used. In the case of the R_{int} the difference is more significant, about 20% higher for CF electrodes. As some authors have suggested [76], these differences could be related to morphological parameters of the electrode microstructure, such as roughness. It should be noted that CF electrodes (Figure 4 e and f), present fibres with larger diameters and a disorderly and heterogeneous distribution, while CM and CC have smaller fibre

diameters (approximately 50% lower), placed homogeneously. Smaller fibres, being properly placed, can improve the contact between the electrode and the ceramic surface [9].

As far as the activation overpotential is concerned, the lowest values were for CF cathodes. This suggests that ORR reaction is favored in carbon felt. In fact, the trend is in line with the results of the kinetic analysis (Table 2). The CF2.5 shows the lowest activation overpotential, and also the highest exchange current density for the oxygen reduction reaction. Although further analysis would be required, the composition of the carbon materials can be the cause of the different behavior between them, since kinetic parameters depend on the electrochemical reaction, electrode material and electrolyte composition. [77]. The presence of graphitic carbon and carbon surface oxides could be responsible, respectively, of increasing the conductivity and the hydrophilic character of the material, as previously reported for CM [9].

The coulombic efficiency varied between 10.7% and 16.5% depending on the cathode used. These values are in line with other works for MFC with clay separators and carbonaceous electrodes without catalyst: 18.5 % [44], 5.8-7.06% [41], 7.69-6.39% [73] and 5.10 % [78]. Despite its internal resistance, the CF5 has the best CE and maximum power values. An increment of power when increasing the thickness of carbon felt electrodes was identified. This behavior has been previously reported in literature for MFC with a Separator Electrode Configuration [79]. The reason could be that the higher thickness probably allows a larger active surface area, or a higher density of active centers where reaction takes place [80].

On the basis of the previous analysis, quite comparable performances of the different materials are obtained: no one stands out against the others for all the parameters. The differences between them may be related to the resistance associated with the way the electrode surface couples to the membrane wall, morphology, composition of the carbonaceous material, the presence of impurities, etc. Therefore, in order to choose the best candidate, an economic analysis was necessary, especially if large-scale real applications of MFCs are considered.

The cost-analysis was done following a procedure proposed in literature.[9]. The approach was based on determining the most cost-effective material, i.e. the material with the lowest cost per energy produced ($€\cdot mA^{-1}$). Calculations were done considering the current produced at 0.5 V. According to Table 5, CF5 showed the best electrochemical performance, 10% higher than CM. However, it was also the most expensive material, concretely 160-200%

higher than the others. Taking this into account, it was found that the most cost-effective material is the CM with a ratio of 0.25 €·mA^{-1}, followed by the CC (0.35€·mA^{-1}). In the work of Santoro et al.[9], CM also appears as the most cost-effective support when compared to Carbon Veil and Carbon Cloth. There are two aspects that are worth noting in this work. First, Carbon Felt is not included, but according to our results a worse ratio than CM is expected, even comparing with the materials of the Santoro's work. Secondly, the cost/produced current ratios are considerably lower than those calculated in the present study. This latter depends on the materials supplier. In any case, the observed trend is equivalent to that obtained by Santoro and other authors [12], which confirms the suitability of the use of CM as cathodic support from a performance-cost perspective.

Table 5. Cost Analysis of cathodic materials

Cost-Effectiveness				
	CC	**CM**	**CF2.5**	**CF5**
$I_{0,5\ V}$ (mA·m^{-2})	107	156	120	172
€·m^{-2}	37 €	38.5	47	74
S (cm^2)		37.25		
I at 0.5 V (mA)	0.398	0.581	0.447	0.641
€·mA^{-1}	**0.35**	**0.25**	**0.39**	**0.43**

Finally, these results bring to the selection of CM as most convenient support for the subsequent deposition of the CuO-based catalyst.

3.4 Performance of the catalyst supported electrodes

The homogeneity of the catalyst coating can be seen in Figure 6: over the whole cathode surface (a) and in a specific fibre (b). The uniform morphology is the result of a precise spraying process. If the dimensions of the fibres before (7μm) and after (19 μm) the deposition of the catalyst are compared, it is obtained that the thickness of the catalytic layer should be approximately 6 μm.

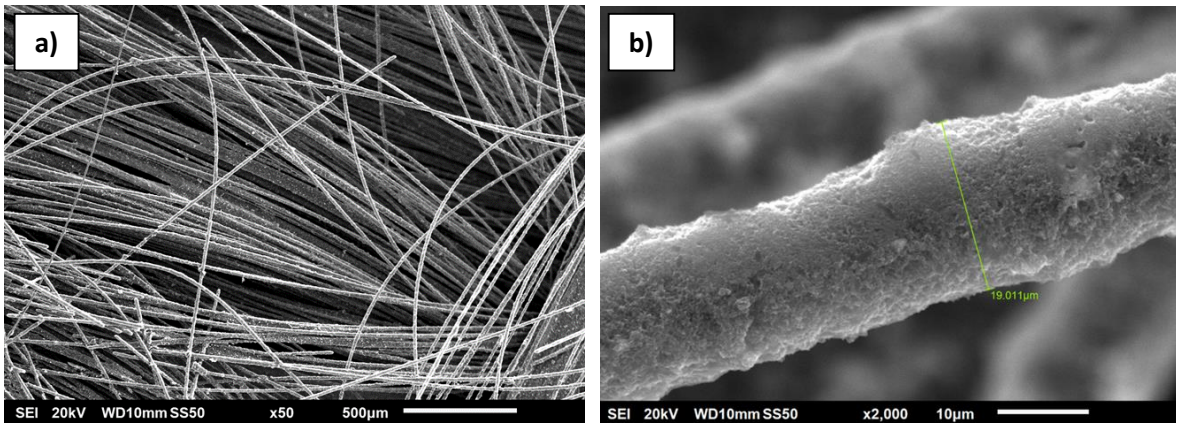

Fig. 6. SEM micrographs of CM-CuO: a) x50 b) x2000 magnification.

CM-CuO cathodes were used in the previous described cell (section 2) where Tafel curves for ORR were derived and compared with those obtained for a CM-Pt electrode (Figure 7).

As we expected, the CM-Pt cathode resulted the best performing (inset, Figure 7); however, noticeably higher catalytic activity was obtained with CM-CuO, compared with that measured with CM, as it is well visible.

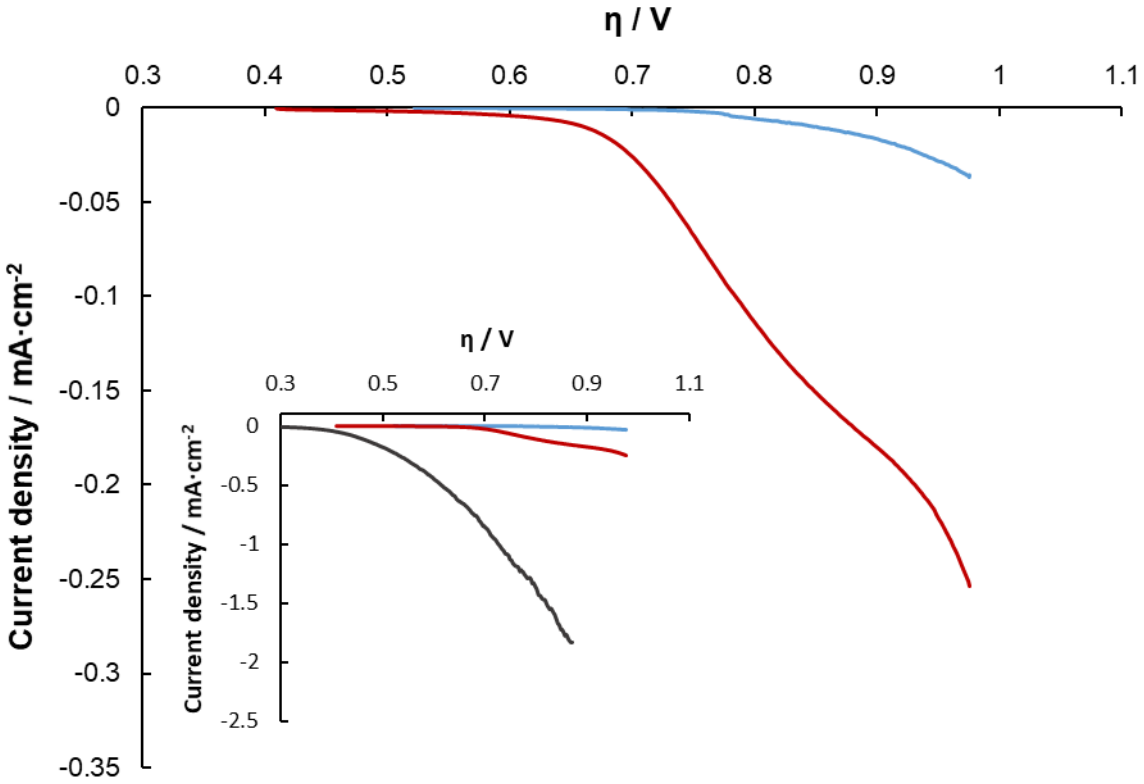

Fig. 7. Trend of current density vs overpotential measured in a three-electrode cell with CM (blue curve) and CM-CuO (red curve) electrodes. Inset: the curve of Pt electrode (black) is reported as a comparison.

Two different plateaus in the low and high overpotential regions can be observed with CM-CuO, and attributed to ORR and hydrogen evolution which, in aqueous solution, becomes prevailing at the highest cathodic potentials. On these bases, Tafel parameters were derived from the first region (in the range of overpotentials between 0.6 V and 0.7 V), at which the linear trend of η *vs log(i*) was observed. Values of i_o and *b* derived from Tafel plots for CM, CM-CuO, and CM-Pt are resumed in Table 6.

Table 6. Tafel parameters calculated for the different cathodic materials.

Cathode	**b ($mV \cdot dec^{-1}$)**	**i_0 ($mA \cdot cm^{-2}$)**
CM	60	8.0×10^{-9}
CM-CuO	62	4.57×10^{-7}
CM-Pt	63	2.21×10^{-4}

As the *b* values are concerned, the same mechanism seems to occur at the three kinds of samples, which involves 2 electrons. Actually, two Tafel slopes may generally be observed for ORR on a Pt electrode surface [81], at high and low overpotential, with Tafel slopes of 60 $mV \cdot dec^{-1}$ and 120 $mV \cdot dec^{-1}$, respectively. This difference was attributed to various mechanisms which occur on a pure Pt or on Pt/PtO surface. At pure Pt, the first electron transfer is the rate determining step, resulting in a Tafel slope of 120 $mV \cdot dec^{-1}$, while on Pt/PtO surface, the rate determining step is a pseudo 2-electron transfer, which gives a Tafel slope of 60 $mV \cdot dec^{-1}$.

As expected, due to the different catalytic activity of the samples, a big difference is obtained between the values of i_0, which are hardly comparable with data from literature: the values may vary widely, depending primarily on the morphology of the catalyst, and on its amount, as well as on temperature.

The performances of the CM-CuO catalyst are better compared in Figure 8 a) where polarization curves are reported related to the cell in which CM or CM-CuO were used as cathode. Data of power density are compared with those obtained without catalyst in Figure 8 b where data are presented as a function of the external resistance.

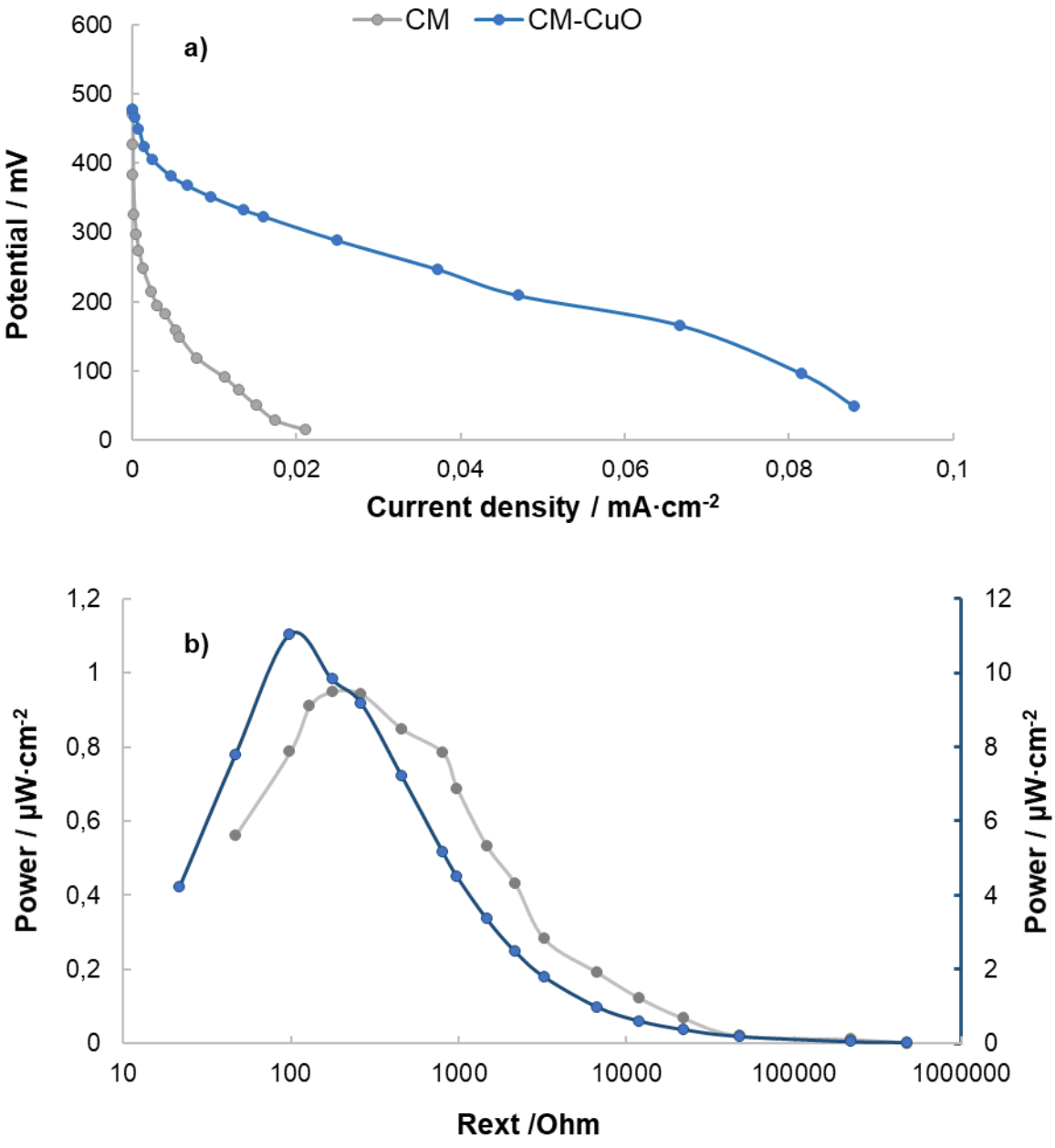

Fig. 8. Effect of the CuO catalyst on: a) polarization curves; (b) power curves as a function of the different external loads (data for CM-CuO are reported in secondary axis).

Also, in this case, the better performance of the catalyst is well visible from both the higher value of maximum power, with an increase of an order of magnitude, but also from the minimum value of R_{ext} at which this maximum is obtained.

Unfortunately, the comparison with other Cu based electrodes tested in other works is not trivial. As previously mentioned, the performance of MFC will depend on multiple factors (geometry, type of separator, electrodes, etc.), and it is very difficult to compare data generated under such different conditions. For these reasons, to contextualize our results with the advances reported in the literature, in Table 7 we provide an overview of different non-precious metals investigated in several MFC set-ups, mainly based on Cu. It is worth noting that only few recent works consider the application of Cu based catalyst to Ceramic-MFC. This shows that the application of these catalysts in ceramic cells has hardly been studied.

Table 7. Bibliographic overview of works in which Cu-based catalysts are used in cathode for ORR in MFC.

Catalyst	**Cathode Preparation Method**	**Cathode/ Anode**	**MFC Configuration**	**Separator**	**MDP ($mW \cdot m^{-2}$)**	**MP-Pt (%)**	**Ratio Vs Control**	**Ref.**
$Cu_{0.30}Co_{0.70}Co_2O_4$	-	CC/GC	SC	Nafion	567.58	87.6	-	[82]
$Cu_{0.92}Co_{2.08}O_4$	Rolling method	SS M/CF	MF-SC	-	1895	-	2.13	[83]
Cu2O	Rolling-press method	SS M/CF	MF-SC	-	1390	-	1.6	[24]
CuxO	Brushed	SS M/CF	SC	-	118.2	98.5	3.1	[84]
CuxO	Rolling-press method + Electrodeposition	SS M/CF	SC	-	1550	-	1.8	[22]
CuxO	Electrodeposition	CC/CF	DC	-	308.69	-	2.5	[26]
Cu Sn	Manual deposition	SS M/CF	SC	Nafion	470	101	5.05	[85]
Cu/Zn	-	CF/CF	TCMFC	Montmorillonite - Clay	75.1	68.2	3.9	[86]

CuO	Spraying	CM/CF	TCMFC	Clay	110	54.45	9.1	This Study

MDP: Maximum Power Density; MP-Pt: Maximum Power versus Pt (%); CC: Carbon Cloth; SS-M: Stainless Steel Mesh; CF: Carbon Felt; CM: Carbon Mesh; SC: Single Chamber; MF-SC: Membrane free Single Chamber; DC: Double Chamber; TCMFC: Tubular Ceramic Microbial Fuel Cell;

From Table 7, it can be seen that, lately, attention has been gained by the spinel-type catalysers for MFC [20]. However, because of the aim of reducing costs, recently alternative low-cost Cu based catalysts are being tested [86]. Another important aspect is the great difference in terms of power response between non-separator, Nafion and ceramic membrane cells. The significant influence of the separator over the overall performance of the cell is here evidenced, with values in the range of 2000-1000 $mW \cdot m^{-2}$ for membrane-less systems, 500 $mW \cdot m^{-2}$ for Nafion cells and 120-80 $mW \cdot m^{-2}$ for Ceramic-MFCs. This trend is not specific to copper catalysts. For example, Co spinel catalysts MFCs reported power densities of 1770.8 $mW \cdot m^{-2}$ [19] when used without membrane, and 176.9 $mW \cdot m^{-2}$ [59] with ceramic membrane. In the present study the Ceramic-MFC, within a CM-CuO cathode reported a power density value of 110 $mW \cdot m^{-2}$, which is much lower compared to membrane-less cells. But if Ceramic-MFCs are considered, our C-MFC with the CM-CuO cathode showed a power density 46% higher than that observed by Das et al. [86] for a ceramic cell with a bimetallic low-cost CuZn catalyst-Carbon Felt support cathode. Furthermore, the CM-CuO cathode presented in this study, showed the highest ratio against the control sample (i.e. the ratio between performances of cell with CM-CuO cathode and cell without catalyst), more than 9 times higher, which contrasts to usually reported values, in the range between 2-4. It is noteworthy to point out that, usually, the electric response when working with carbon supported catalysts, should be due to the sum of catalyst action and carbon particles (Carbon Black, Activated Carbon, etc)[13]. In our study the control sample is just CM material, but the Cu-based catalyst contains also a 50% wt.% of carbon black, which is well known to increase the cathode conductivity [9], and even to have a considerable catalytic activity [87]. However, its influence is expected to be lower than in the case of Activated Carbon (AC) catalyst supported cathodes, since carbon black catalytic activity is lower than AC [88].

On the other hand, since power densities can vary greatly depending on different aspects (cell geometry, electrode materials, etc.), a good alternative to compare the MFCs performances is the percentage out of the maximum power reached by platinum-type cathodes [82]. This concept represents the performance displayed by a certain catalyst

respect to Pt, which is the standard catalyst for the ORR reaction in fuel cells. In this case our cathode showed a 54.7% power response regarding those of Pt cathode (Table 7). This behaviour could be related to the catalyst loading. In the present study we used a certain CuO catalyst loading (3.5 $mg \cdot cm^{-2}$), but probably it is not the optimal one for this material. It may be taken in consideration, that non-Pt catalysts may compensate their lower activity with higher loadings, which is convenient since their prize is considerably lower than Pt. In fact, loadings can vary in the range 1-5< $mg \cdot cm^{-2}$ for Cu catalysts in C-MFCs [85]. Thus, further studies would be needed to identify the suitable loading of CuO catalyst.

Finally, a CE of 24.85% was obtained for the cell working with CM-CuO. This represent an increment of more than 100% respect CM electrode. Only a few studies working on MFC with Cu based catalysts report CE values. In these cases the coulombic efficiency varied between 28-55% for MFCs without membrane or using CEM membranes [84][85][60].

3.5 Long-term operation

The response of a catalyst during long operating times without deterioration is one of the most desired characteristics of the new materials. Especially in low-cost or Pt-free materials, since longer life time has a positive implication on the profitability. Moreover, stability over time can be an advantage over Pt, since it has been widely reported the significant decrement of Pt catalyst activity and yield, after several weeks or months of operation [13][14].

In the present work, the fabricated cathode has been tested for more than 6 months. Figure S5 depicts the E (V) Vs t (h) evolution for a Ceramic microbial fuel cell with Cu-CM cathode connected to an external resistance of 150 Ω. After 4 months working with CM as cathode, the new CM-CuO cathode was assembled in the cell. During the first days a strong increment on potential output was observed, which stabilized in the following 25-30 days, and then progressively dropped from 150 mV up to an almost stable value of 130 mV, with some low peaks of 120 mV approximately. This variability could be related to the worsening of electrical contact between electrodes and current collectors.

During the studied period, the decay in the electrical response is estimated at around 21.5 % in terms of E (mV). In Figure 9 polarization curves for day 130 and 370 are presented. It worth noting that CM-CuO is assembled in the C-MFC after 120 day of operation, as shown in Figure S5. The maximum power density values decreased from 110 $mW \cdot m^{-2}$ to 77.7 $mW \cdot m^{-2}$ between days 130 and 370, respectively (corresponding to days 10 and 250 of CM-

CuO operation). This result corresponds to a degradation rate of 29.4% after more than 6 months.

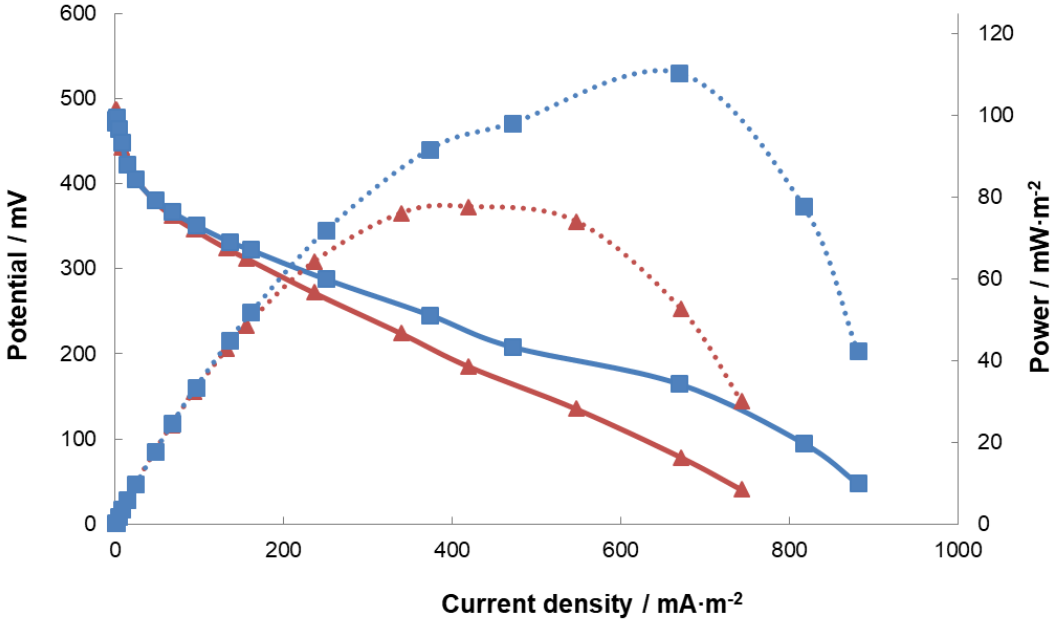

Fig. 9. Polarization and power density curves for a C-MFC with CM-CuO cathode during long term operation. (Blue lines: day 130; Red lines: day 370)

On the other hand, comparison of long-term results with existent literature becomes limited. Firstly, the majority of the studies correspond to initial cathode performances, in "clean" operational conditions and not in long-term experiments [13]. Secondly, there are few studies that analyse cathodic performance in long-term test of more than 30 days. And besides, most of these works report membrane-less configuration.

If works with durability test of several months are considered, several authors reported the degradation of different cathodes: after 4.5 months of operation, Zhang et al. [88], observed a degradation of more than 60% in terms of power density for Pt/C cathodes, in contrast a decay of almost 12% verified with FeEDTA/Activated Carbon cathodes. Gadghe and Granghear [78] reported a decrease of power after 12 months within 41% on Ceramic-MFC with MnO_2/CB cathode. These authors demonstrated that the cause of the decline was chemical fouling as a result of synthetic wastewater. Also, for C-MFCs with AC/Carbon Veil air cathodes, a decay of 20% was confirmed after 350 days [3]. From these studies it is evidenced that the main causes of power decay over time operation are: biofouling in cathodes or separators, catalyst activity loss, catalytic coating detachment, etc.[89][78].

In our case, after more than 250 days of operation with the CM-CuO cathode, some white salt crystals were evident (Figure S6a), indicating the existence of fouling phenomena. The presence of these salts was previously found by other authors working with C-MFC and it was related to electro-osmotic drag phenomena [50,78]. This "chemical fouling" can saturate the separator porous and reduce the cathode active area, resulting in the increment of internal resistance of the cell and a decay of power. Figure S6 (b and c) presents SEM images of different zones of sample surface. Two points are relevant: the presence of large and small deposits covering the surface, and the loss of catalyst from the fibres (Figure S6 d). The latter becomes more evident when the new CM-CuO sample is compared with the long-term one (SEM images in Figures 6 and 6S, respectively). EDS analysis of the cathode surface (Figure S6 e) confirmed the existence of Na, P, Mg, etc. mainly coming from the anolyte.

3.6 Cost Analysis

Accounting for the costs of clay (17 €·ton^{-1}, source: http://de.statista.com/), electrical energy (0,16 €·kW·h^{-1}, calculated as average of commercial energy tariffs in Italy and Spain), catalyst (200 €·kg^{-1}, source: Sotacarbo SpA), Nafion (738 €·L) and electrode supports (85.5 €·m^{-2}, sum of anode and cathode prices, reported in Figure 5), and adapting the procedure proposed by Chakraborty et al. [4], the fabrication costs of 0.37€ and 0.86 € have been calculated for the membrane and the whole MFC, respectively, if they are produced singularly, by the lab procedure indicated in section 2. However, costs strongly decrease if large scale production is considered. Based on previous studies, the cost of such a system was estimated at between >1€ [47] and 19.73€ [5] depending on the used materials.

Of note, in the present study, energy cost is one of the most influent term in determining the membrane cost; however, multiple samples can be produced in a single cycle: up to 145 samples can be lodged in the oven, which allow to produce about 1 m^2 of membrane, energetic consumption being the same. In this way cost of the membrane passes from 54,6 €·m^{-2} to 0.43 €·m^{-2}, that accounts for 3% of the cost of the cell, as compared to CEM membranes that generally represents about 40% [22]-60 % [5] of the total fabrication cost. And costs could further decrease if higher amount of carbon material is bought for the electrode supports.

A complete cost analysis requires a comparison with other MFC cases. However, direct comparison with other MFC studies is not feasible due to their differing designs, constituent materials, and operational conditions [90]. On the other hand, usually MFC works focus on

the optimization of one component [59], and commonly the cost-analysis are limited to the commercial prize of this component or the total costs of the lab scale cell. Furthermore, some MFC fabrication costs (such as energy consumption, machining and drilling costs, etc.) are usually not taken into consideration, yet they are relevant if the scaling up and commercialization of MFC technology is to be addressed. For all these reasons, making a comparison with other low-cost systems it is a complex task. Moreover, the scope of this "low-cost" concept is not clear from the literature, since there is no uniformity or standardization in the presentation of economic analyses. This makes difficult to know the true cost of a system, and only a few studies present complete cost analyses [5]. In such a multidisciplinary technology, it would be desirable to try to cover the entire manufacturing process costs of a system, in order to make a more realistic estimation.

In this respect, a complete cost analysis was reported by Chakraborty et col. for a MFC equipped with Nafion or with membranes produced by biochar [4]. This procedure is very detailed and allows a wide performance-cost evaluation with an industrial production perspective. We followed and adapted this approach to our cost-analysis. The obtained results are reported in Table 8 and compared with these authors' values [4].

Table 8. Comparison between cost and performances of the MFC in the present work and those from literature.

Item of comparison	**This work**	**MFC-biochar** [4]	**MFC-Nafion**[4]
Cost of 1 m^2 membrane (€)	0.43	67.7	2560
Cost of 1 MFC, including membrane and reactor fabrication (€)	0.49	6.4	11
Power density per unit of membrane utilized (mW m^{-2})	60.92	41	-
Power density ($W \cdot m^{-3}$)	2.74	1.14	1.62
Power density achieved per unit cost of MFC fabrication ($W \cdot m^{-3} \cdot €^{-1}$)	5.183	0.198	0.133

Power achieved per unit cost of membrane utilized ($W \cdot €^{-1}$)	0.14	0.3	0.012
Cost of Membrane per unit of electricity generated ($€ \cdot mW^{-1}$)	0.007	2	54

Power density of the system presented in this study is not so high when compared with other Ceramic-MFC which usually reports values between: 1.16-7.55 $W \cdot m^{-3}$ [46][58]. Nevertheless, the optimization of manufacturing process makes able to obtain a very low-cost membrane with a production cost of 0.43 $€ \cdot m^{-2}$. This contrast with the ceramic membrane costs shown in literature, in the range of 1.7-402.6 $€ \cdot m^{-2}$ [90]. As consequence, reduced fabrication costs result in one of the cheapest C-MFC reported, with a cell unit cost of 0.49 €. This allows to strongly improve the power output, obtaining a value of 140 $mW \cdot €^{-1}$ (per unit cost of membrane), which is, to the best of our knowledge, one of the highest value reported in literature for ceramic microbial fuel cell (regardless of geometry), which ranges between 24.57-107.3 $mW \cdot €^{-1}$, according with a recent work [90]. These cost-analysis results confirm the convenience of the optimization strategy and the use of Slip-Casting as separator fabrication method and validate the proposed C-MFC as one of the most cost-effective designs developed at the moment.

4. Conclusions

In the present work, a novel cost-effective Ceramic Microbial Fuel cell has been presented and extensively characterized. A suitable combination of consolidated low-cost manufacturing techniques and inexpensive materials allowed the fabrication of a system able to work for more than 6 months with a unitary cost of 0.49€/cell and a power output of 140 $mW \cdot €^{-1}$ (per unit cost of membrane).

The application of slip-casting for the manufacture of C-MFC tubular separators has been successfully reported for the first time. It has been demonstrated that it is an accurate, versatile and economical process, which allows the control of geometry, thickness and porosity in a cost efficient and simple way. The potential of this methodology has been shown by the manufacture of 1.5 mm tubular separators for MFCs. So far, the lowest thickness in this type of separators, with the possibility of being reduced even further, may be a subject for future work.

In addition, a cathode composed of a carbonaceous support and a low-cost CuO-based catalyst has been manufactured and used in C-MFC for the first time. Among the carbonaceous supports tested, Carbon Mesh has proven to be the most cost-effective material with a ratio of 0.25 €·mA^{-1}. The new CM-CuO cathode showed a power 9 times higher than the CM, and more than 40 % higher than other Cu based cathodes for C-MFCs studied in the literature. Although being far from the performance of Pt-cathodes, the CM-CuO cathode has shown acceptable performance in long-term tests. During the first 35 days the potential barely decreased by 6.2%, and after 250 days the value was reduced by 21.5% (29.4% in terms of power density). This is an advantageous aspect compared to Pt, which has shown strong losses of activity during the first month (almost 50%[88]). Therefore, in the long-term operation CM-CuO cathode can provide a technical and economic advantage. Although the results are very encouraging, our group continues working to optimize the manufactured cathode by analyzing aspects such as: catalyst loading, carbon black response, coating method, etc.

Finally, an extensive cost analysis has shown that the proposed system, combining a Pt-Free cathode and a ceramic cell represents a very competitive alternative from an economic point of view. In the specific case of the ceramic membrane, the price of the separators built by slip-casting, on a laboratory scale, is reduced by more than half compared to that reported in the literature for ceramic cells. Moreover, the energy optimization during the manufacturing of the ceramic membranes has reduced the cost of this component to 3% of the whole cell. This has meant a drastic reduction in the cost of each unit C-MFC, reaching one of the lowest values reported to date.

The obtained results confirm that the combination of ceramic separators and Pt-free catalysts has great future potential, both from a long-term performance and cost perspective. The proposed process of slip casting can be an effective method to synthesize membranes and, at the same time, ensure that its specific chemical-physical characteristics (such as thickness and porosity), are designed in a controlled manner, thus responding to the needs recently exhibited by the scientific community in the field of C-MFC [50].

Acknowledgments

This study was financially supported by Ministerio de Ciencia, Innovación y Universidades (MCIU, Spain), Junta de Comunidades de Castilla-La Mancha (JCCM, Spain) and European Regional Development Fund (ERDF). The authors would like to express their gratitude to

Dr. Mira Sulonen for their valuable technical support with biofilm samples preparation for pyrosequencing. Gema Sevilla is thanked for help with Scanning Electron Microscopy measurements

References

[1] Leong JX, Daud WRW, Ghasemi M, Liew K Ben, Ismail M. Ion exchange membranes as separators in microbial fuel cells for bioenergy conversion: A comprehensive review. Renew Sustain Energy Rev 2013;28:575–87. https://doi.org/10.1016/j.rser.2013.08.052.

[2] Do MH, Ngo HH, Guo W, Chang SW, Nguyen DD, Liu Y, et al. Microbial fuel cell-based biosensor for online monitoring wastewater quality: A critical review. Sci Total Environ 2020;712. https://doi.org/10.1016/j.scitotenv.2019.135612.

[3] Gajda I, Obata O, Jose Salar-Garcia M, Greenman J, Ieropoulos IA. Long-term bio-power of ceramic microbial fuel cells in individual and stacked configurations. Bioelectrochemistry 2020;133:107459. https://doi.org/10.1016/j.bioelechem.2020.107459.

[4] Chakraborty I, Das S, Dubey BK, Ghangrekar MM. Novel low cost proton exchange membrane made from sulphonated biochar for application in microbial fuel cells. Mater Chem Phys 2020;239:122025. https://doi.org/10.1016/j.matchemphys.2019.122025.

[5] Ge Z, Technology ZH-ESWR&, 2016 undefined. Long-term performance of a 200 liter modularized microbial fuel cell system treating municipal wastewater: treatment, energy, and cost. PubsRscOrg n.d.

[6] Rismani-Yazdi H, Carver SM, Christy AD, Tuovinen OH. Cathodic limitations in microbial fuel cells: An overview. J Power Sources 2008;180:683–94. https://doi.org/10.1016/j.jpowsour.2008.02.074.

[7] Xin S, Shen J, Liu G, Chen Q, Xiao Z, Zhang G, et al. Electricity generation and microbial community of single-chamber microbial fuel cells in response to Cu2O nanoparticles/reduced graphene oxide as cathode catalyst. Chem Eng J 2020;380. https://doi.org/10.1016/j.cej.2019.122446.

[8] Cheng S, Liu H, Logan BE. Increased performance of single-chamber microbial fuel

cells using an improved cathode structure. Elsevier n.d. https://doi.org/10.1016/j.elecom.2006.01.010.

[9] Santoro C, Artyushkova K, Gajda I, Babanova S, Serov A, Atanassov P, et al. Cathode materials for ceramic based microbial fuel cells (MFCs). Int J Hydrogen Energy 2015;40:14706–15. https://doi.org/10.1016/j.ijhydene.2015.07.054.

[10] Palanisamy G, Jung HY, Sadhasivam T, Kurkuri MD, Kim SC, Roh SH. A comprehensive review on microbial fuel cell technologies: Processes, utilization, and advanced developments in electrodes and membranes. J Clean Prod 2019;221:598–621. https://doi.org/10.1016/j.jclepro.2019.02.172.

[11] Deng Q, Li X, Zuo J, Ling A, Logan BE. Power generation using an activated carbon fiber felt cathode in an upflow microbial fuel cell. J Power Sources 2010;195:1130–5. https://doi.org/10.1016/j.jpowsour.2009.08.092.

[12] Luo Y, Wei B, Liu G, Zhang R, Logan BE. Power generation using carbon mesh cathodes with different diffusion layers in microbial fuel cells. J Power Sources 2011;196:9317–21. https://doi.org/10.1016/j.jpowsour.2011.07.077.

[13] Santoro C, Serov A, Stariha L, Kodali M, Gordon J, Babanova S, et al. Iron based catalysts from novel low-cost organic precursors for enhanced oxygen reduction reaction in neutral media microbial fuel cells. Energy Environ Sci 2016;9:2346–53. https://doi.org/10.1039/c6ee01145d.

[14] Zhang X, Pant D, Zhang F, Liu J, He W, Logan BE. Long-Term Performance of Chemically and Physically Modified Activated Carbons in Air Cathodes of Microbial Fuel Cells. ChemElectroChem 2014;1:1859–66. https://doi.org/10.1002/celc.201402123.

[15] Zhang L, Fu G, Zhang Z. Simultaneous nutrient and carbon removal and electricity generation in self-buffered biocathode microbial fuel cell for high-salinity mustard tuber wastewater treatment. Bioresour Technol 2019;272:105–13. https://doi.org/10.1016/j.biortech.2018.10.012.

[16] Santoro C, Babanova S, Erable B, Schuler A, Atanassov P. Bilirubin oxidase based enzymatic air-breathing cathode: Operation under pristine and contaminated conditions. Bioelectrochemistry 2016;108:1–7. https://doi.org/10.1016/j.bioelechem.2015.10.005.

[17] Chorbadzhiyska E, Bardarov I, Hubenova Y, Mitov M. Graphite–Metal Oxide Composites as Potential Anodic Catalysts for Microbial Fuel Cells. Catalysts 2020;10:796. https://doi.org/10.3390/catal10070796.

[18] Bhowmick GD, Das S, Verma HK, Neethu B, Ghangrekar MM. Improved performance of microbial fuel cell by using conductive ink printed cathode containing Co3O4 or Fe3O4. Electrochim Acta 2019;310:173–83. https://doi.org/10.1016/j.electacta.2019.04.127.

[19] Huang Q, Zhou P, Yang H, Zhu L, Wu H. In situ generation of inverse spinel CoFe2O4 nanoparticles onto nitrogen-doped activated carbon for an effective cathode electrocatalyst of microbial fuel cells. Chem Eng J 2017;325:466–73. https://doi.org/10.1016/j.cej.2017.05.079.

[20] Wang J, Li K, Zhang L, Ge B, Liu Y, Yang T, et al. Temperature-depended Cu0.92Co2.08O4 modified activated carbon air cathode improves power output in microbial fuel cell. Int J Hydrogen Energy 2017;42:3316–24. https://doi.org/10.1016/j.ijhydene.2016.09.104.

[21] Zhou DL, Feng JJ, Cai LY, Fang QX, Chen JR, Wang AJ. Facile synthesis of monodisperse porous Cu2O nanospheres on reduced graphene oxide for non-enzymatic amperometric glucose sensing. Electrochim Acta 2014;115:103–8. https://doi.org/10.1016/j.electacta.2013.10.151.

[22] Liu Z, Li K, Zhang X, Ge B, Pu L. Influence of different morphology of three-dimensional CuxO with mixed facets modified air-cathodes on microbial fuel cell. Bioresour Technol 2015;195:154–61. https://doi.org/10.1016/j.biortech.2015.06.077.

[23] Sri Abirami Saraswathi MS, Rana D, Divya K, Gowrishankar S, Sakthivel A, Alwarappan S, et al. Highly permeable, antifouling and antibacterial poly(ether imide) membranes tailored with poly(hexamethylenebiguanide) coated copper oxide nanoparticles. Mater Chem Phys 2020;240:122224. https://doi.org/10.1016/j.matchemphys.2019.122224.

[24] Zhang X, Li K, Yan P, Liu Z, Pu L. N-type Cu2O doped activated carbon as catalyst for improving power generation of air cathode microbial fuel cells. Bioresour Technol 2015;187:299–304. https://doi.org/10.1016/j.biortech.2015.03.131.

[25] Yang T, Li K, Liu Z, Pu L, Zhang X. One-Step Synthesis of Hydrangea-like Cu 2 O @ N-doped Activated Carbon as Air Cathode Catalyst in Microbial Fuel Cell . J Electrochem Soc 2017;164:F270–5. https://doi.org/10.1149/2.0401704jes.

[26] Dong F, Zhang P, Li K, Liu X, Zhang P. Nano copper oxide-modified carbon cloth as cathode for a two-chamber microbial fuel cell. Nanomaterials 2016;6:1–12. https://doi.org/10.3390/nano6120238.

[27] Castresana P, Martinez S, Freeman E, … SE-E, 2019 undefined. Electricity generation from moss with light-driven microbial fuel cells. Elsevier n.d.

[28] Bakonyi P, Koók L, Kumar G, … GT-J of M, 2018 undefined. Architectural engineering of bioelectrochemical systems from the perspective of polymeric membrane separators: A comprehensive update on recent progress. Elsevier n.d.

[29] Liu H, Logan BE. Electricity generation using an air-cathode single chamber microbial fuel cell in the presence and absence of a proton exchange membrane. Environ Sci Technol 2004;38:4040–6. https://doi.org/10.1021/es0499344.

[30] Lawati M Al, Jafary T, … MB-B and, 2019 undefined. A mini review on biofouling on air cathode of single chamber microbial fuel cell; prevention and mitigation strategies. Elsevier n.d.

[31] González-Rodríguez L, Rodríguez J, Rojas N, Sánchez-Molina M, Campana R, Rodríguez L. Nafion-metallic oxides membranes for intermediate temperature PEMFC. WHEC 2016 - 21st World Hydrog. Energy Conf. 2016, Proc., 2016, p. 806–8.

[32] Hernández-Flores G, Poggi-Varaldo HM, Solorza-Feria O. Comparison of alternative membranes to replace high cost Nafion ones in microbial fuel cells. Int J Hydrogen Energy 2016;41:23354–62. https://doi.org/10.1016/j.ijhydene.2016.08.206.

[33] Dhar BR, Lee HS. Membranes for bioelectrochemical systems: challenges and research advances. Environ Technol (United Kingdom) 2013;34:1751–64. https://doi.org/10.1080/09593330.2013.822007.

[34] Salar-García M, Sources II-J of P, 2020 undefined. Optimisation of the internal structure of ceramic membranes for electricity production in urine-fed microbial fuel

cells. Elsevier n.d.

[35] Daud S, Kim B, Ghasemi M, technology WD-B, 2015 undefined. Separators used in microbial electrochemical technologies: current status and future prospects. Elsevier n.d.

[36] Khudzari J, Kurian J, … BT-B, 2018 undefined. Bibliometric analysis of global research trends on microbial fuel cells using Scopus database. Elsevier n.d.

[37] Yousefi V, Mohebbi-Kalhori D, Samimi A. Ceramic-based microbial fuel cells (MFCs): A review. Int J Hydrogen Energy 2017;42:1672–90. https://doi.org/10.1016/j.ijhydene.2016.06.054.

[38] Pasternak G, Greenman J, Ieropoulos I. Comprehensive Study on Ceramic Membranes for Low-Cost Microbial Fuel Cells. ChemSusChem 2016;9:88–96. https://doi.org/10.1002/cssc.201501320.

[39] Salar-García MJ, Walter XA, Gurauskis J, Fernández A de R, Ieropoulos I. Effect of iron oxide content and microstructural porosity on the performance of ceramic membranes as microbial fuel cell separators. Electrochim Acta 2020:137385. https://doi.org/10.1016/j.electacta.2020.137385.

[40] Winfield J, Greenman J, Huson D, Ieropoulos I. Comparing terracotta and earthenware for multiple functionalities in microbial fuel cells. Bioprocess Biosyst Eng 2013;36:1913–21. https://doi.org/10.1007/s00449-013-0967-6.

[41] Behera M, Ghangrekar MM. Electricity generation in low cost microbial fuel cell made up of earthenware of different thickness. Water Sci Technol 2011;64:2468–73. https://doi.org/10.2166/wst.2011.822.

[42] Jimenez I, Greenman J, hydrogen II journal of, 2017 undefined. Electricity and catholyte production from ceramic MFCs treating urine. Elsevier n.d.

[43] Salar-García MJ, de Ramón-Fernández A, Ortiz-Martínez VM, Ruiz-Fernández D, Ieropoulos I. Towards the optimisation of ceramic-based microbial fuel cells: A three-factor three-level response surface analysis design. Biochem Eng J 2019;144:119–24. https://doi.org/10.1016/j.bej.2019.01.015.

[44] Ghadge AN, Ghangrekar MM. Development of low cost ceramic separator using mineral cation exchanger to enhance performance of microbial fuel cells.

Electrochim Acta 2015;166:320–8. https://doi.org/10.1016/j.electacta.2015.03.105.

[45] Ahilan V, Wilhelm M, International KR-C, 2018 undefined. Porous polymer derived ceramic (PDC)-montmorillonite-H3PMo12O40/SiO2 composite membranes for microbial fuel cell (MFC) application. Elsevier n.d.

[46] Me M, Energy MB-IJ of H, 2019 undefined. Tubular ceramic performance as separator for microbial fuel cell: A review. Elsevier n.d.

[47] Behera M, Jana PS, Ghangrekar MM. Performance evaluation of low cost microbial fuel cell fabricated using earthen pot with biotic and abiotic cathode. Bioresour Technol 2010;101:1183–9. https://doi.org/10.1016/j.biortech.2009.07.089.

[48] Ajayi FF, Weigele PR. A terracotta bio-battery. Bioresour Technol 2012;116:86–91. https://doi.org/10.1016/j.biortech.2012.04.019.

[49] Salar-García MJ, Ortiz-Martínez VM, Gajda I, Greenman J, Hernández-Fernández FJ, Ieropoulos IA. Electricity production from human urine in ceramic microbial fuel cells with alternative non-fluorinated polymer binders for cathode construction. Sep Purif Technol 2017;187:436–42. https://doi.org/10.1016/j.seppur.2017.06.025.

[50] You J, Wallis L, Radisavljevic N, Pasternak G, Sglavo VM, Hanczyc MM, et al. A Comprehensive Study of Custom-Made Ceramic Separators for Microbial Fuel Cells: Towards "Living" Bricks. MdpiCom n.d. https://doi.org/10.3390/en12214071.

[51] Winfield J, Gajda I, Greenman J, Ieropoulos I. A review into the use of ceramics in microbial fuel cells. Bioresour Technol 2016;215:296–303. https://doi.org/10.1016/j.biortech.2016.03.135.

[52] Sui J, Liu J. An Electrolyte-supported SOFC Stack Fabricated by Slip Casting Technique. IopscienceIopOrg 2019;7:633–7. https://doi.org/10.1149/1.2729146.

[53] Hedayat N, Du Y, Reviews HI-R and SE, 2017 undefined. Review on fabrication techniques for porous electrodes of solid oxide fuel cells by sacrificial template methods. Elsevier n.d.

[54] Zhang L, He HQ, Kwek WR, Ma J, Tang EH, Jiang SP. Fabrication and characterization of anode-supported tubular solid-oxide fuel cells by slip casting and dip coating techniques. J Am Ceram Soc 2009;92:302–10.

https://doi.org/10.1111/j.1551-2916.2008.02852.x.

[55] Boussemghoune M, Chikhi M, Balaska F, Ozay Y, Dizge N, Kebabi B. Preparation of a Zirconia-Based Ceramic Membrane and Its Application for Drinking Water Treatment. MdpiCom n.d. https://doi.org/10.3390/sym12060933.

[56] Elyassi B, Sahimi M, science TT-J of membrane, 2007 undefined. Silicon carbide membranes for gas separation applications. Elsevier n.d.

[57] Alimoradi A, Moradzadeh A, Bakhtiari MR. Methods of water saturation estimation: Historical perspective. J Pet Gas Eng 2011;2:45–53.

[58] Khalili H-B, Mohebbi-Kalhori D, Afarani MS. Microbial fuel cell (MFC) using commercially available unglazed ceramic wares: Low-cost ceramic separators suitable for scale-up. Int J Hydrogen Energy 2017;42:8233–41. https://doi.org/10.1016/j.ijhydene.2017.02.095.

[59] Das I, Noori MT, Bhowmick GD, Ghangrekar MM. Synthesis of bimetallic iron ferrite Co0.5Zn0.5Fe2O4 as a superior catalyst for oxygen reduction reaction to replace noble metal catalysts in microbial fuel cell. Int J Hydrogen Energy 2018;43:19196–205. https://doi.org/10.1016/j.ijhydene.2018.08.113.

[60] Noori M, Bhowmick G, … BT-M, 2018 undefined. Application of low-cost Cu–Sn bimetal alloy as oxygen reduction reaction catalyst for improving performance of the microbial fuel cell. CambridgeOrg n.d.

[61] Rago L, Guerrero J, Baeza JA, Guisasola A. 2-Bromoethanesulfonate degradation in bioelectrochemical systems. Bioelectrochemistry 2015;105:44–9. https://doi.org/10.1016/j.bioelechem.2015.05.001.

[62] Sevda S, Dominguez-Benetton X, Vanbroekhoven K, De Wever H, Sreekrishnan TR, Pant D. High strength wastewater treatment accompanied by power generation using air cathode microbial fuel cell. Appl Energy 2013;105:194–206. https://doi.org/10.1016/j.apenergy.2012.12.037.

[63] Fricke K, Harnisch F, Schröder U. On the use of cyclic voltammetry for the study of anodic electron transfer in microbial fuel cells. Energy Environ Sci 2008;1:144–7. https://doi.org/10.1039/b802363h.

[64] Harnisch F, Freguia S. A basic tutorial on cyclic voltammetry for the investigation

of electroactive microbial biofilms. Chem - An Asian J 2012;7:466–75. https://doi.org/10.1002/asia.201100740.

[65] Marsili E, Sun J, Bond DR. Voltammetry and growth physiology of Geobacter sulfurreducens biofilms as a function of growth stage and imposed electrode potential. Electroanalysis 2010;22:865–74. https://doi.org/10.1002/elan.200800007.

[66] Khalili HB, Mohebbi-Kalhori D, Afarani MS. Microbial fuel cell (MFC) using commercially available unglazed ceramic wares: Low-cost ceramic separators suitable for scale-up. Int J Hydrogen Energy 2017;42:8233–41. https://doi.org/10.1016/j.ijhydene.2017.02.095.

[67] Du Z, Li H, Gu T. A state of the art review on microbial fuel cells: A promising technology for wastewater treatment and bioenergy. Biotechnol Adv 2007;25:464–82. https://doi.org/10.1016/j.biotechadv.2007.05.004.

[68] Yang X, Ma X, Wang K, Wu D, Lei Z, Feng C. Eighteen-month assessment of 3D graphene oxide aerogel-modified 3D graphite fiber brush electrode as a high-performance microbial fuel cell anode. Electrochim Acta 2016;210:846–53. https://doi.org/10.1016/j.electacta.2016.05.215.

[69] Rago L, Zecchin S, Marzorati S, Goglio A, … LC-, 2018 undefined. A study of microbial communities on terracotta separator and on biocathode of air breathing microbial fuel cells. Elsevier n.d.

[70] Li M, Zhou M, Tian X, Tan C, … CM-B, 2018 undefined. Microbial fuel cell (MFC) power performance improvement through enhanced microbial electrogenicity. Elsevier n.d.

[71] Park H, Kim B, Kim H, Kim H, Kim G, Anaerobe MK-, et al. A novel electrochemically active and Fe (III)-reducing bacterium phylogenetically related to Clostridium butyricum isolated from a microbial fuel cell. Elsevier n.d.

[72] Ben Liew K, Daud WRW, Ghasemi M, Leong JX, Su Lim S, Ismail M. Non-Pt catalyst as oxygen reduction reaction in microbial fuel cells: A review. Int J Hydrogen Energy 2014;39:4870–83. https://doi.org/10.1016/j.ijhydene.2014.01.062.

[73] Ghadge AN, Sreemannarayana M, Duteanu N, Ghangrekar MM. Influence of ceramic separator's characteristics on microbial fuel cell performance. J

Electrochem Sci Eng 2014;4:315–26. https://doi.org/10.5599/jese.2014.0047.

[74] Song C, Zhang J. Electrocatalytic oxygen reduction reaction. PEM Fuel Cell Electrocatal. Catal. Layers Fundam. Appl., Springer London; 2008, p. 89–134. https://doi.org/10.1007/978-1-84800-936-3_2.

[75] Rossi R, Cario BP, Santoro C, Yang W, Saikaly PE, Logan BE. Evaluation of Electrode and Solution Area-Based Resistances Enables Quantitative Comparisons of Factors Impacting Microbial Fuel Cell Performance. Environ Sci Technol 2019;53:3977–86. https://doi.org/10.1021/acs.est.8b06004.

[76] Santoro C, Artyushkova K, … SB-B, 2014 undefined. Parameters characterization and optimization of activated carbon (AC) cathodes for microbial fuel cell application. Elsevier n.d.

[77] Raghavulu SV, Suresh Babu P, Goud RK, Subhash GV, Srikanth S, Mohan SV. Bioaugmentation of an electrochemically active strain to enhance the electron discharge of mixed culture: process evaluation through electro-kinetic analysis. PubsRscOrg n.d. https://doi.org/10.1039/c1ra00540e.

[78] Ghadge AN, Ghangrekar MM. Performance of low cost scalable air-cathode microbial fuel cell made from clayware separator using multiple electrodes. Bioresour Technol 2015;182:373–7. https://doi.org/10.1016/j.biortech.2015.01.115.

[79] Ahn Y, Logan BE. Altering Anode Thickness To Improve Power Production in Microbial Fuel Cells with Different Electrode Distances. ACS Publ 2012;27:271–6. https://doi.org/10.1021/ef3015553.

[80] Kinoshita K. Mass-Transfer Study of Carbon Felt, Flow-Through Electrode. J Electrochem Soc 1982;129:1993. https://doi.org/10.1149/1.2124338.

[81] Wakabayashi N, Takeichi M, Itagaki M, Uchida H, Watanabe M. Temperature-dependence of oxygen reduction activity at a platinum electrode in an acidic electrolyte solution investigated with a channel flow double electrode. J Electroanal Chem 2005;574:339–46. https://doi.org/10.1016/j.jelechem.2004.08.013.

[82] Ortiz-Martínez VM, Salar-García MJ, Touati K, Hernández-Fernández FJ, de los Ríos AP, Belhoucine F, et al. Assessment of spinel-type mixed valence Cu/Co and Ni/Co-based oxides for power production in single-chamber microbial fuel cells.

Energy 2016;113:1241–9. https://doi.org/10.1016/j.energy.2016.07.127.

[83] Wang J, Li K, Zhang L, Ge B, Liu Y, … TY-IJ of, et al. Temperature-depended Cu0. 92Co2. 08O4 modified activated carbon air cathode improves power output in microbial fuel cell. Elsevier n.d.

[84] Ghasemi M, Daud WRW, Rahimnejad M, Rezayi M, Fatemi A, Jafari Y, et al. Copper-phthalocyanine and nickel nanoparticles as novel cathode catalysts in microbial fuel cells. Int J Hydrogen Energy 2013;38:9533–40. https://doi.org/10.1016/j.ijhydene.2013.01.177.

[85] Noori MT, Bhowmick GD, Tiwari BR, Ghangrekar OM, Ghangrekar MM, Mukherjee CK. Carbon Supported Cu-Sn Bimetallic Alloy as an Excellent Low-Cost Cathode Catalyst for Enhancing Oxygen Reduction Reaction in Microbial Fuel Cell. J Electrochem Soc 2018;165:F621–8. https://doi.org/10.1149/2.0271809jes.

[86] Das I, Das S, Ghangrekar MM. Application of bimetallic low-cost CuZn as oxygen reduction cathode catalyst in lab-scale and field-scale microbial fuel cell. Chem Phys Lett 2020;751. https://doi.org/10.1016/j.cplett.2020.137536.

[87] Marinho B, Ghislandi M, Tkalya E, Technology CK-P, 2012 undefined. Electrical conductivity of compacts of graphene, multi-wall carbon nanotubes, carbon black, and graphite powder. Elsevier n.d.

[88] Xia X, Zhang F, Zhang X, Liang P, Huang X, Logan BE. Use of Pyrolyzed Iron Ethylenediaminetetraacetic Acid Modified Activated Carbon as Air−Cathode Catalyst in Microbial Fuel Cells. ACS Publ 2013;5:7862–6. https://doi.org/10.1021/am4018225.

[89] Rossi R, Yang W, Zikmund E, Pant D, Logan BE. In situ biofilm removal from air cathodes in microbial fuel cells treating domestic wastewater. Bioresour Technol 2018;265:200–6. https://doi.org/10.1016/j.biortech.2018.06.008.

[90] Yousefi V, Mohebbi-Kalhori D, of AS-IJ, 2020 undefined. Start-up investigation of the self-assembled chitosan/montmorillonite nanocomposite over the ceramic support as a low-cost membrane for microbial fuel cell. Elsevier n.d.